ISSN 8755-6839

SCIENCE OF **TSUNAMI HAZARDS**

Journal of Tsunami Society International

Volume 35 **Number 3** **2016**

LANDSLIDE-TYPE TSUNAMI MODELLING BASED ON THE NAVIER - STOKES EQUATIONS

A.S. Kozelkov [1,2)], A.A. Kurkin[2)], E.N. Pelinovsky[2-4)], E.S. Tyatyushkina[1)], V.V. Kurulin[1)], N.V. Tarasova[1)]

1) Russian Federal Nuclear Center, All-Russian Research Institute of Experimental Physics, Sarov, Russia
2) Nizhny Novgorod State Technical University n.a. R. Alekseyev, Nizhny Novgorod, Russia
3) Institute of Applied Physics, Nizhny Novgorod, Russia
4) National Research University – Higher School of Economics, Moscow, Russia

ABSTRACT

The paper presents a unified computing technology for all stages of landslide-type tsunami. The computing technology is based on the numerical solution of the Navier – Stokes equations for multiphase flows. The method of numerical solution of the Navier – Stokes equations uses a fully implicit algorithm. This algorithm removes stiff restrictions on the time steps and allows simulating a tsunami propagation in arbitrarily large water basins. The basic sampling equation formulas, coefficient types as well as the basic steps of the computational procedure are presented. The landslide is modeled by a single phase with its density and viscosity, which is separated by the interface from water and air phases. A parallel algorithm of the method implementation based on an algebraic multigrid method is proposed for the effective usage of the method to calculate the tsunami in large water areas. The multigrid method of implementation is based on algorithms of global level and cascading collection. These algorithms do not impose restrictions on the scale parallelization and allow the use of the proposed technology in petaflop class systems. It shows the possibility of

simulating all the stages of the landslide-type tsunamis: generation, propagation and runup. The verification of the method is carried out by using the tests provided by the experimental data. The mechanism of bathymetric data accounting and the technology of constructing three-dimensional grid models are described. The results of the comparison with the non-linear dispersion theory are presented for the historical tsunami that resulted from a volcanic eruption on the island of Montserrat, the Caribbean. The results of this comparison are in good agreement.

1. INTRODUCTION

Tsunami database contains more than 2,200 registered events in the world and more than 9,000 observations of wave heights on a shore (http://tsun.sscc.ru/hiwg). More than 10% of them are tsunamis generated by underwater and aerial landslides, and 5% are generated by volcanic sources, to be more precise, by pyroclastic flows formed as a result of a volcanic explosion. According to the accumulated data, tsunamis generated by landslides have the highest runup heights, which can reach several hundred meters. The most famous landslide-type tsunamis are events in Alaska (Lituya Bay) (1853, 1936, 1958), Norway (1936) and Greenland (2000) (Rabinovich et al., 2003; Fine et al., 2005; Papadopoulos & Kortekaas, 2005). The greatest tsunami wave height of 60 meters was observed in Lituya Bay on 10 July, 1958 with a maximum splash in the bay itself 525 meters. The review of historical landslides and tsunamis generated by them can be found in (Langford, 2007; Papadopoulos & Kortekaas, 2005).

Waves excited by underwater and aerial landslides achieve the maximum possible runup directly near the source at a distance of 10-15 km along the coastline (Papadopoulos & Kortekaas, 2005). However, the tsunami of this kind can propagate significantly further. They can keep their destructive potential for hundreds of kilometers.

Tsunamigenic landslides can be divided into three types: aerial, partially submerged in the water and submarine. The initial position of the landslide is the basis for selecting physical and mathematical models suitable to describe tsunami generation and propagation. It is advisable to use a three-phase system: fluid-air-landslide to describe aerial and partially underwater landslides, whereas for underwater landslides it is enough to use a two-phase or a two-layer model with different density layers. The landslide itself is modeled by a non-deformable rigid body or a system of such bodies as well as by incompressible fluid or a separate layer with its own values of density and viscosity coefficients (Fedotova et al, 2004; Watts & Grilli, 2003; Heinrich et al, 1998; Imamura & Imteaz, 1995; Zahibo et al, 2010; Nikolkina et al, 2010; Didenkulova et al, 2010, 2011).

Surface waves generated by landslides are specific in their own way. The formation of the wave in the coastal zone takes a fairly long period of time comparable to the time of the landslide movement. The characteristic landslide size is often comparable with the depth. Unlike the tsunamis of seismic origin the landslide-type tsunamis are shorter (Dutykh & Dias, 2009), which requires considering wave dispersion. To simulate these waves nonlinear-dispersive shallow water equations are used which are able to reproduce the dispersion. These equations are solved by finite-difference methods built on the basis of the second-order accuracy schemes (Watts & Grilli, 2003). However, these systems include mixed higher order derivatives. Due to that, building efficient numerical algorithms to solve them it is

not a trivial task. The use of nonlinear dispersive equations for simulating landslide tsunamis is discussed in (Fedotova et al, 2004; Gusev et al., 2013).

It is worth noting that the type of landslide tsunami is paid enough attention to. A large series of experimental studies (Langford, 2007; Watts & Grilli, 2003; Sælevik et al., 2009; Fritz et al., 2009; Horrillo et al., 2013; Mohammed & Frits 2010; Mohammed, 2010)[1], and some theoretical works (Langford, 2007; Papadopoulos& Kortekaas, 2005; Fedotova et al., 2004; Watts & Grilli, 2003; Imamura & Imteaz, 1995; Dutykh & Dias, 2009; Gusev et al., 2013; Beizel et al., 2011; Harbitz et al., 2006) have allowed substantial progress in the development of numerical methods for tsunami calculation.

Besides experimental data, there are analytical solutions available for calibration and testing the developed methods (Pelinovsky, 2003; Okal & Synolakis, 2003; Didenkulova et al., 2010). Numerous articles discuss the results of historical landslide type tsunami simulation (Heinrich et al, 1998; Rabinovich et al, 2003; Fine et al, 2005; Sælevik et al, 2009; Fritz et al, 2009; Horrillo et al, 2013; Macías et al, 2015). The study of the various effects accompanying this phenomenon are described in (Pelinovsky, 2003; Watts & Grilli, 2003; Fedotova et al, 2004; Harbitz et al, 2006; Didenkulova et al, 2010; Beizel et al, 2011).

According to (Lynett, 2010) two approaches must be used to describe landslide-type tsunami formation correctly: the solution of fully 3D hydrodynamics equations or a simplified system based on them which is the result of depth integration. Depth integration, in fact, eliminates the vertical coordinate and reduces a 3D system to 2D, which serves as the basis for an NLSW (nonlinear shallow-water) class models. This class of models is well established in modeling seismic tsunami propagation over long distances. The use of NLSW models for landslide-type tsunami leads to the incorrect description of wave form and propagation time. It is caused by shorter wave generation in comparison with seismic sources (Lynett, 2010). For the majority of landslide-type tsunami it is more reasonable to use the Boussinesq equations, although they also have limitations (Watts et al, 2003). The use of 3D models to generate a landslide-type tsunami is reduced to the use of special systems on the basis of the Laplace equation (Cecioni & Bellotti, 2010 ; Grilli et al, 2002). An attempt to use three-dimensional models based on the fully Navier-Stokes equations is represented in a few works (Horrillo et al, 2013; Ma et al, 2013; Liu et al., 2005) due to their computational cost. However, in recent years there has been a significant increase in computing power and their affordability, so the development and application of these models is becoming an urgent task. The use of the Navier-Stokes equations together with the equation for calculating deformable landslide motion (Ma et al., 2013). LES (Large Eddy Simulation) approach to this class of problems (Liu et al., 2005) seems uncertain due to very strict requirements for the used numerical schemes and the calculation of the cascade transfer of turbulent kinetic energy for vortex structures of different scales (Kozelkov et al., 2016; Kozelkov & Kurulin, 2015). In (Horrillo et al., 2013) a simplified 3D model was used to generate the landslide-type tsunami source in the Gulf of Mexico. The use of a complete 3D model to calculate all tsunami waves stages including the runup seems promising enough. At present, to calculate the propagation (including formation) and runup the multi-layer models are used (Lynett & Liu, 2005): one model for propagation, and the other for the runup calculation. The review of physical

[1]Paper [14] gives an extensive bibliography on the experimental and analytical studies of landslide-type tsunami.

and mathematical models currently used to simulate the landslide-type tsunami is presented in (Mohammed, 2010).

The main difficulty in using the Navier-Stokes equations in scientific and industrial applications is their significant computational cost. The current system study is aimed at developing the methods of hydrodynamic calculation acceleration as well as at improving their accuracy (Volkov et al, 2013; Kozelkov et al, 2013; Kozelkov et al., 2016).

This paper presents a computed technique for landslide-type tsunami calculation on the basis of a fully implicit method of solution fully 3D Navier-Stokes equations which describe multiphase flows. The proposed method significantly weakens the demand for the time steps, which is one of the main advantages in the simulation of tsunami propagation over long distances. The fully implicit scheme also proves very stable. The algorithm for accelerating the convergence of the proposed method using multigrid technologies is presented in the paper. The basic sample formulae, the stages of the computational procedure and the algorithm for the bathymetric data accounting are given. The efficiency of the technology is tested on the known experimental data. The possibility of using the computed technology to calculate all landslide tsunami stages and to simulate tsunami in any part of the World Ocean is demonstrated in the paper. Section 2 presents the basic model equations and methodology of their numerical solution. The results of the proposed methodology validation in problems of tsunami generation which is the result of surface and underwater landslides having experimental data are given in Section 3. Section 4 presents the technology of three-dimensional grid model construction in the World Ocean with the detailed areas of the slide, runup and tsunami propagation. Section 5 describes the technology of calculation acceleration based on the algebraic multigrid method. Section 6 presents the landslide tsunami simulation results using different approaches from the source and with the simulated pyroclastic flow slide within the Navier - Stokes equations. The obtained results are summarized in Section 7.

2. BASIC MODEL EQUATIONS AND NUMERICAL SOLUTION METHOD

Let us consider the “air-water” system as a set of two incompressible media separated by the interface. We will use the one-velocity approximation, in which the continuity equation and the equation of momentum conservation are the same for both water and air. These equations are solved for the resultant medium, the properties of which are linearly dependent on the volume fraction (Hirt & Nichols, 1981). This approach is quite widespread and gives good results in solving problems with a free surface (Ubbink, 1997) including those for tsunami waves (Horrillo et al, 2013; Kozelkov et al., 2015; Kozelkov & Pelinovsky, 2016). In the framework of this approximation the motion is described by the Navier-Stokes equations, including equations of continuity, momentum conservation, as well as the equation for the volume fraction of the phases (Kolev, 2007; Volkov & Emelyanov, 2008):

$$\begin{cases} \nabla \cdot \mathbf{u} = 0, \\ \dfrac{\partial}{\partial t} \sum\limits_k \alpha^{(k)} \rho^{(k)} \mathbf{u} = -\nabla \cdot \sum\limits_k \left(\alpha^{(k)} \rho^{(k)} \mathbf{u}\mathbf{u} \right) + \nabla \cdot \sum\limits_k \left(\alpha^{(k)} \mu^{(k)} \nabla \mathbf{u} \right) - \nabla p + \sum\limits_k \alpha^{(k)} \rho^{(k)} \mathbf{g}, \\ \dfrac{\partial}{\partial t} \alpha^{(k)} \rho^{(k)} + \nabla \cdot \left(\alpha^{(k)} \rho^{(k)} \mathbf{u} \right) = 0, \end{cases} \qquad (1)$$

here $\mathbf{u}$ is a three-dimensional velocity vector $\rho^{(k)}$ is density of k-phase, and $\alpha^{(k)}$ is its volume fraction ($\sum\limits_k \alpha_k = 1$), p is pressure, $\mu^{(k)}$ is molecular viscosity of k-phase, $\mathbf{g}$ is gravity acceleration. This system is solved directly without the use of Reynolds averaging and the subsequent closure of the turbulence model. This allows solving turbulent structures, the minimum scale of which is determined by the grid resolution.

System sampling (1) can be carried out by any known method. The best choice is the finite volume method (Ubbink, 1997; Kozelkov & Kurulin, 2015) which possesses good conservative properties and enables sampling complex computational areas on arbitrary unstructured grids with cells of arbitrary shape. The main difficulty in the numerical solution of the system (1) is to determine the connection of the pressure field with the velocity field. The procedure of matching the pressure field with a rate field should lead to the simultaneous satisfaction of the continuity and momentum conservation equations. The most common methods are SIMPLE type methods based on pressure correction procedure, or the principle of splitting the unknown quantities (Ferziger & Peric, 2001; Kozelkov et al, 2013). For the SIMPLE-procedure the equation for the volume fraction and the mass forces is omitted, a cell P with the faces $f = nb(P)$ is considered, and the system of equations (1) is written in a discrete form:

$$\begin{cases} \sum\limits_{f=nb(P)} \mathbf{u}_f^n S_f = 0, \\ \sum\limits_k \alpha^{(k)} \rho^{(k)} \dfrac{\mathbf{u}^n - \mathbf{u}^{n-1}}{\tau} V = - \sum\limits_{f=nb(P)} \sum\limits_k \alpha^{(k)} \rho_f^{(k)} \mathbf{u}_f^{n-1} \mathbf{u}_f^n S_f + \sum\limits_{f=nb(P)} \sum\limits_k \alpha^{(k)} \mu_f^{(k)} \nabla \mathbf{u}_f^n S_f - \\ - \sum\limits_{f=nb(P)} p_f^n S_f + \sum\limits_k \alpha^{(k)} \rho^{(k)} \mathbf{g} V, \end{cases} \qquad (2)$$

where n is time layer, τ is time step, S_f is the area of the interface f between the control volumes of the computational grid (Fig. 1), $\mathbf{u}_f$ – is the value of the velocity on the edge (hereinafter, the index f means the affiliation of a value to a face), $nb(P)$ – is the number of cell edges (in this case, cell ***P***), see Fig. 1.

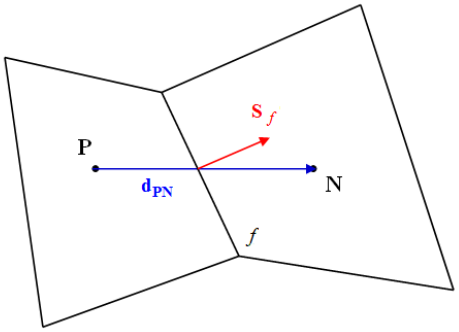

Fig. 1. Adjacent control volumes of the computational grid

The solution of system (1) by the SIMPLE algorithm assumes that the equation for the transfer of volume fractions (n – 1) for the volume fraction $\alpha^{(n)} = 1 - \sum_{k \neq n} \alpha^{(k)}$ of phases k is solved separately from continuity and momentum conservation equations. In the classic formulation of the SIMPLE algorithm the connection of velocity and pressure is carried out semi-implicitly. It takes place through the use of pressure from the previous iteration step, which often leads to slow the solution convergence. To improve the efficiency of work and the SIMPLE algorithm convergence modifications that best adapt to the velocity and pressure fields are developed. One such modification is a combined algorithm for solving velocity and pressure (Chen & Przekwas, 2010). The combination is done by implicit sampling of the pressure gradient and mass flow in the conservation of momentum and continuity equations. That helps to avoid the steps of predictor and corrector. Thus obtained implicit coefficients are summed into a single diagonally dominant matrix solved by using multigrid methods (Volkov et al, 2013; Kozelkov et al, 2013; Kozelkov et al, 2016; Tai & Zhao, 2003).

For the combined algorithm system solutions (1) the system of equations (2) is rewritten in the form of:

$$\begin{cases} \sum\limits_{f=nb(P)} \left\{ \overline{\mathbf{u}_f^n} + \overline{\mathbf{D}_f} \left[\left(\overline{\nabla p_f^{n-1}} \right) - \left(\nabla p_f^n \right) \right] \right\} S_f = 0, \\ \sum\limits_k \alpha^{(k)} \rho^{(k)} \dfrac{\mathbf{u}^n - \mathbf{u}^{n-1}}{\tau} V = - \sum\limits_{f=nb(P)} \sum\limits_k \alpha^{(k)} \rho_f^{(k)} \mathbf{u}_f^{n-1} \mathbf{u}_f^n S_f + \sum\limits_{f=nb(P)} \sum\limits_k \alpha^{(k)} \mu_f^{(k)} \nabla \mathbf{u}_f^n S_f - \\ - \sum\limits_{f=nb(P)} p_f^n S_f + \sum\limits_k \alpha^{(k)} \rho^{(k)} \mathbf{g} V, \end{cases} \quad (3)$$

here, the "upper line" indicates that the edge value is obtained by interpolation of the adjacent control volumes. The continuity equation in the system (3) uses the Rhie-Chow correction (Rhie & Chow, 1983) which levels the difference of pressure gradient approximation in the continuity and momentum conservation equations. The amendment also links the velocity and pressure fields at the simultaneous solution of continuity and motion equations.

To implement the fully implicit algorithm for the solution of (3) can be rewritten in its algebraic form:

$$\begin{cases} \sum\limits_{j\in\{p,u,v,w\}} a_P^{pj} j_P + \sum\limits_{N=NB(P)} \left[\sum\limits_{j\in\{p,u,v,w\}} a_N^{pj} j_N \right] = b_P^p, \\ \sum\limits_{j\in\{p,u,v,w\}} a_P^{ij} j_P + \sum\limits_{N=NB(P)} \left[\sum\limits_{j\in\{p,u,v,w\}} a_N^{ij} j_N \right] = b_P^i, \; i = \{u,v,w\}. \end{cases} \tag{4}$$

The summation over the index «*j*» for the first equation of the system (4) – continuity equation, gives general matrix coefficients to calculate the pressure in the control volume of the discrete model. These coefficients are:

$$a_N^{pp} = \frac{\left(\overline{\mathbf{D}_f}\mathbf{S}_f\right)\mathbf{S}_f}{\mathbf{S}_f \cdot \mathbf{d}_{PN}}, \quad a_P^{pp} = -\sum_{f=nb(P)} a_f^{pp},$$

$$a_N^{pu} = \left(1-\lambda_f\right)S_f^x, \quad a_N^{pv} = \left(1-\lambda_f\right)S_f^y, \quad a_N^{pw} = \left(1-\lambda_f\right)S_f^z, \tag{5}$$

$$a_P^{pu} = \sum_{f=nb(P)} \left|\lambda_f S_f^x\right|, \; a_P^{pv} = \sum_{f=nb(P)} \left|\lambda_f S_f^y\right|, \; a_P^{pw} = \sum_{f=nb(P)} \left|\lambda_f S_f^z\right|.$$

For these coefficients, a non-orthogonal correction algorithm is used (Jasak, 1996), allowing to correct the calculation on arbitrary unstructured grids. The formula of calculating the edge pressure by using linear interpolation from the values in the center cells is also used (Ferziger & Peric, 2001):

$$p_f = \lambda_f p_P + \left(1-\lambda_f\right)p_N. \tag{6}$$

For the first equation of the system (4) the right side has the form:

$$b_p^p = \sum_{f=nb(P)} \overline{\mathbf{D}_f \nabla p_f} \cdot \mathbf{S}_f - \overline{\mathbf{D}_f} \nabla p_f \cdot \left(\mathbf{S}_f - \frac{\mathbf{S}_f \cdot \mathbf{S}_f}{\mathbf{S}_f \cdot \mathbf{d}_{PN}} \mathbf{d}_{PN} \right). \tag{7}$$

The summation over the index «*i*» for the second equation of the system (4) – for the conservation momentum equation - gives the total matrix system coefficients to calculate the velocity component:

$$a_N^{uu} = a_N^{vv} = a_N^{ww} = \sum_k \alpha_f^{(k)} \mu_f \frac{\mathbf{S}_f \cdot \mathbf{S}_f}{\mathbf{S}_f \cdot \mathbf{d}_{PN}} + \min\left(0, \sum_k \alpha_f^{(k)} \rho_f^{(k)} S_f\right). \tag{8}$$

The first term of (8) refers to the diffusion term, and the total matrix system coefficients have the form:

$$a_N^{up} = (1-\lambda_f)S_f^x,\ a_N^{vp} = (1-\lambda_f)S_f^y,\ a_N^{wp} = (1-\lambda_f)S_f^z,$$
$$a_P^{up} = \sum_{f=nb(P)} \lambda_f S_f^x,\ a_P^{vp} = \sum_{f=nb(P)} \lambda_f S_f^y, a_P^{wp} = \sum_{f=nb(P)} \lambda_f S_f^z. \quad (9)$$

As well as for the coefficients (5), a non-orthogonal correction algorithm for recording is used.

The second term of the expressions (7) is a convective component, which is approximated by any known differential scheme applicable on arbitrary unstructured grids (Volkov et al., 2013; Kozelkov et al, 2015, 2016). Commonly used is an upwind difference (UD) or a counter-flow scheme with linear interpolation (linear upwind differences, LUD), the QUICK scheme, the central difference scheme (CD), the NVD family schemes (Normalized Variable Diagram), a hybrid scheme in which all the above mentioned schemes are mixed with a counter-flow scheme to increase monotony.

Non-stationary term sampling can be carried out by one of the known implicit schemes (Jasak, 1996; Ferziger & Peric, 2001). The contribution of diffusion and convection terms of conservation momentum equations applies to diagonal coefficients of the general matrix system, which, considering the non-stationary sampled term using the Euler scheme, have the form:

$$a_P^{uu} = -\sum_{N=NB(P)} a_N^{uu} + \sum_k \alpha_P^{(k)}\rho_P^{(k)}\frac{V}{\tau},$$
$$a_P^{vv} = -\sum_{N=NB(P)} a_N^{vv} + \sum_k \alpha_P^{(k)}\rho_P^{(k)}\frac{V}{\tau}, \quad (10)$$
$$a_P^{ww} = -\sum_{N=NB(P)} a_N^{ww} + \sum_k \alpha_P^{(k)}\rho_P^{(k)}\frac{V}{\tau}.$$

For the second equation of (4) the right-hand side has the form:

$$b_p^u = \sum_{f=nb(P)} \left[\nabla u \cdot \mu_f \cdot \left(\mathbf{S}_f - \frac{\mathbf{S}_f \cdot \mathbf{S}_f}{\mathbf{S}_f \cdot \mathbf{d}_{PN}}\mathbf{d}_{PN}\right)\right] + \sum_k \alpha_P^{(k)}\rho_P^{(k)}u_P\frac{V}{\tau} + \sum_k \alpha^{(k)}\rho^{(k)}g_x V,$$
$$b_p^v = \sum_{f=nb(P)} \left[\nabla v \cdot \mu_f \cdot \left(\mathbf{S}_f - \frac{\mathbf{S}_f \cdot \mathbf{S}_f}{\mathbf{S}_f \cdot \mathbf{d}_{PN}}\mathbf{d}_{PN}\right)\right] + \sum_k \alpha_P^{(k)}\rho_P^{(k)}v_P\frac{V}{\tau} + \sum_k \alpha^{(k)}\rho^{(k)}g_y V, \quad (11)$$
$$b_p^w = \sum_{f=nb(P)} \left[\nabla w \cdot \mu_f \cdot \left(\mathbf{S}_f - \frac{\mathbf{S}_f \cdot \mathbf{S}_f}{\mathbf{S}_f \cdot \mathbf{d}_{PN}}\mathbf{d}_{PN}\right)\right] + \sum_k \alpha_P^{(k)}\rho_P^{(k)}w_P\frac{V}{\tau} + \sum_k \alpha^{(k)}\rho^{(k)}g_z V.$$

Thus, the combined system of linear algebraic equations of the fully implicit algorithm for the simulation of a multiphase flow is as follows:

$$\begin{bmatrix} a_P^{pp} & a_P^{pu} & a_P^{pv} & a_P^{pw} \\ a_P^{up} & a_P^{uu} & a_P^{uv} & a_P^{uw} \\ a_P^{vp} & a_P^{vu} & a_P^{vv} & a_P^{vw} \\ a_P^{wp} & a_P^{wu} & a_P^{wv} & a_P^{ww} \end{bmatrix} \begin{bmatrix} p_P \\ u_P \\ v_P \\ w_P \end{bmatrix} + \sum_{N=NB(P)} \begin{bmatrix} a_N^{pp} & a_N^{pu} & a_N^{pv} & a_N^{pw} \\ a_N^{up} & a_N^{uu} & a_N^{uv} & a_N^{uw} \\ a_N^{vp} & a_N^{vu} & a_N^{vv} & a_N^{vw} \\ a_N^{wp} & a_N^{wu} & a_N^{wv} & a_{NN}^{ww} \end{bmatrix} \begin{bmatrix} p_N \\ u_N \\ v_N \\ w_N \end{bmatrix} = \begin{bmatrix} b_P^p \\ b_P^u \\ b_P^v \\ b_P^w \end{bmatrix}. \quad (12)$$

This system is written to calculate the total velocity and pressure of the multiphase flow, but it can be generalized in case each phase has its own speed and physical properties such as compressibility and turbulence. These generalizations will be held in further.

To simulate the phase boundaries after solving the system (12), the equation of volume fraction transfer is solved (third equation (1)), which can be solved for (n – 1) the volume fractions of phases. Its sampling by the finite volume method is carried out according to the scheme completely similar to the one used for the conservation momentum equation. To approximate the convective term of volume fraction transfer, equation M-CICSAM scheme (Waclawczyk & Koronowicz, 2008) is used. It refers to a class of compression schemes of high resolution; it ensures the lowest possible thickness of the interface and preserves the volume fraction distribution under parallel transfer and rotation.

In the algebraic form the given system of equations for the k-phase is as follows:

$$a_P^{(k)}\alpha_P^{(k)} + \sum_{N=NB(P)} a_N^{(k)}\alpha_N^{(k)} = b_P^{(k)}. \quad (13)$$

The coefficients of the matrix of the equation implicit solution (13) are of the form:

$$\begin{aligned} a_N^{(k)} &= \min\left(0, u_f^{(n-1)} S_f\right) \quad a_P^{(k)} = -\sum_{N=NB(P)} a_N^{(k)} + \frac{V}{\tau}, \\ b_P^{(k)} &= -u_f^{(n-1)} S_f \cdot \left(\alpha_{MC}^{(k)} - \alpha_{UD}^{(k)}\right) + \frac{V}{\tau}\alpha_P^{(k),n-1}, \end{aligned} \quad (14)$$

where $\alpha_{MC}^{(k)}$, $\alpha_{UD}^{(k)}$ are values of the volume fraction on the edge found by MCICSAM scheme and, the counter-flow scheme, respectively, $\alpha_P^{(k),n-1}$ is the value of the volume fraction on the previous time step. These terms are obtained by a non-orthogonal correction along with sampling.

For the numerical solution the resulting equation system must be supplemented by initial and boundary conditions. On solid walls (such as the bottom of the basin), the pressure and the volume fraction gradient and the speed is zero: $\frac{\partial p}{\partial n} = 0$, $\frac{\partial \alpha_k}{\partial n} = 0$, $\mathbf{u} = 0$.

On the «free» borders static pressure is fixed, velocity and volume fraction gradients are equal to zero: $\frac{\partial u}{\partial n} = 0$, $\frac{\partial v}{\partial n} = 0$, $\frac{\partial w}{\partial n} = 0$, $\frac{\partial \alpha_k}{\partial n} = 0$. In modeling geophysical problems the upper limit should be placed high enough to avoid “spilling” water from the computational domain.

Initially, water and air are at rest: $u_0 = v_0 = w_0 = 0$, the pressure distribution is hydrostatic, i.e. satisfies the equation:

$$\nabla p = \mathbf{g} \sum_k \rho^{(k)} \alpha^{(k)} \ . \tag{15}$$

The volume fraction of phases (e.g. water and air) is determined in accordance with a predetermined level of the free surface position.

The calculation of the landslide movement in this model is carried out by means of a separate phase having its own density and viscosity, as well as water and air, i.e. a three-phase hydrodynamic system is obtained. Additional boundary conditions for landslide modeling are not required; all interactions with the liquid and air are modeled by the corresponding terms of the original system of equations. The fully implicit formulation of the numerical scheme relieves severe restrictions on the time step and ensures the stability of the iterative process at the maximum possible Courant number.

The presented method is implemented in the LOGOS software package - a software product designed to solve conjugated three-dimensional problems of convective heat transfer, aerodynamics and hydrodynamics on parallel computers (Betelin et al, 2014; Kozelkov et al, 2016). The LOGOS software package has successfully been verified and shown quite good results in a series of different hydrodynamic problems (Volkov et al, 2013; Kozelkov et al, 2013; Betelin et al, 2014) including turbulent and unsteady flow calculations (Kozelkov et al, 2015, 2016), as well as tsunami waves of cosmogenic origin (Kozelkov & Pelinovsky, 2016; Kozelkov et al., 2015). All the calculations in this article are conducted by using the LOGOS software package.

3. VERIFICATION OF THE NUMERICAL MODEL

The proposed methodology can be validated by using a number of the available experimental data (Langford, 2007; Watts&Grilli, 2003; Sælevik et al, 2009; Fritz et al, 2009; Horrillo et al, 2013; Mohammed&Frits, 2010; Mohammed, 2010; Chen & Przekwas, 2010; Grilli et al, 2003; Watts, et al., 2001). Here we describe some tests for verification of numerical model.

3.1. Aerial landslide simulation

Figure 2 shows a schematic configuration of experimental tank with a pneumatic installation to generate a tsunami by deformed granular landslides (Fritz et al, 2009; Mohammed & Frits, 2010; Mohammed, 2010).

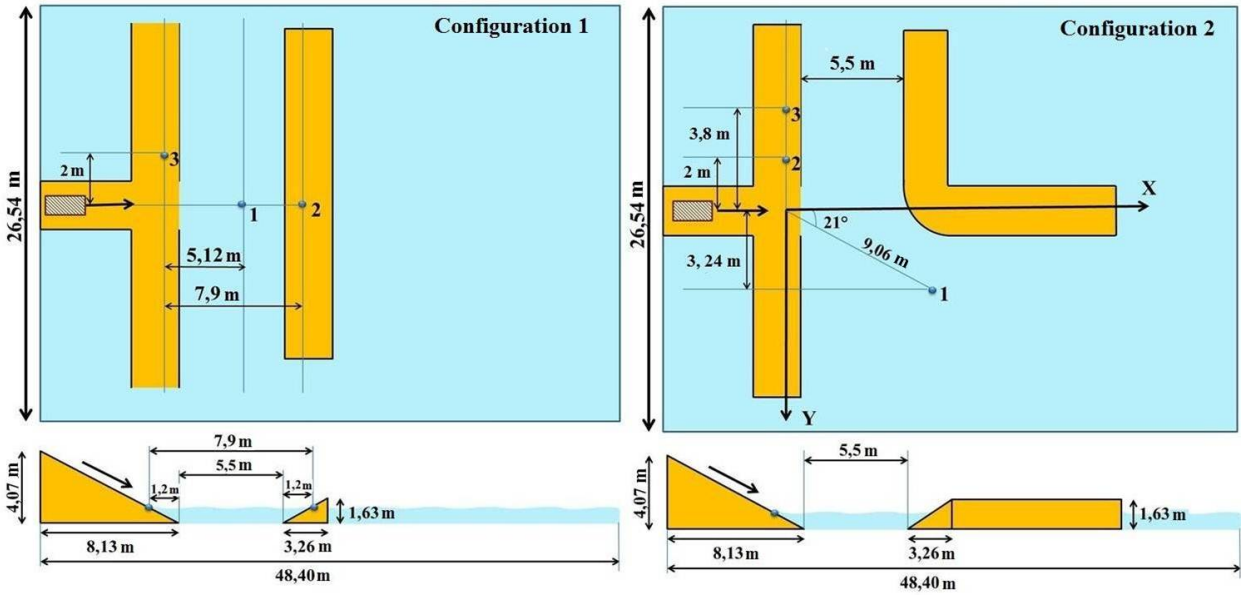

Fig. 2. A tank configuration to study a landslide-type tsunami

(landslide location, tide-gauge location)

The landslide starts its motion along the inclined plane with a predetermined initial velocity of 3.8 m/s. During the experiment the input landslide speed into the water is measured as well as the water displacememnt in some tide-gauge points located in both the "open" water (tide-gauge 1) and in the vicinity of artificial barriers to measure the runup (tide-gauges 2, 3). Tide-gauge 1 in "configuration 1" is located directly in the wave propagation path, and in "configuration 2" it is aimed at measuring the envelope of the barrier wave.

The computational grid consisting of 10 million cells is used for the simulation (Fig. 3). In the area of the landslide and wave propagation the grid has a concentration to describe the motion of the landslide and flow characteristics more accurately.

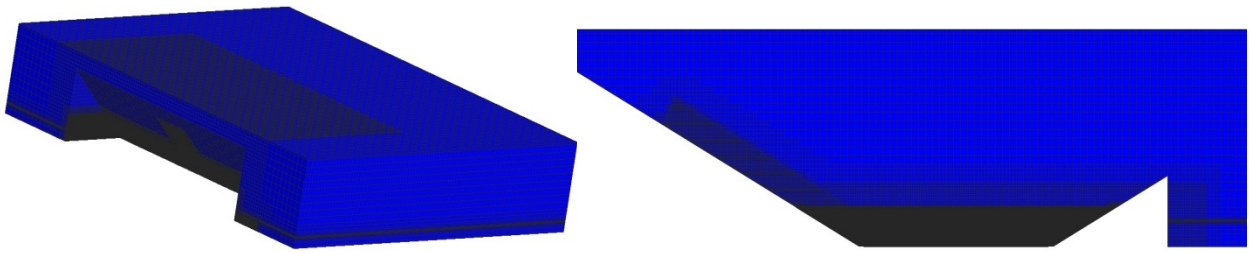

Fig. 3. Grid area (left - a general view, right – the cross section)

The parameters of all three phases: water, air and landslide - are chosen in accordance with the experiment (Table 1). The water depth is 0.6 m. The landslide dimensions constitute 2.1 m × 1.2 m × 0.3 m with its rear edge at a distance of 2.8 m from the top of the inclined plane.

Table 1

Phase characteristics

Phase	Molecular viscosity (kg/m/s))	Density (kg/m^3)
Water	0,001	1000
Air	1,85e-05	1,205
Landslide	26	2600

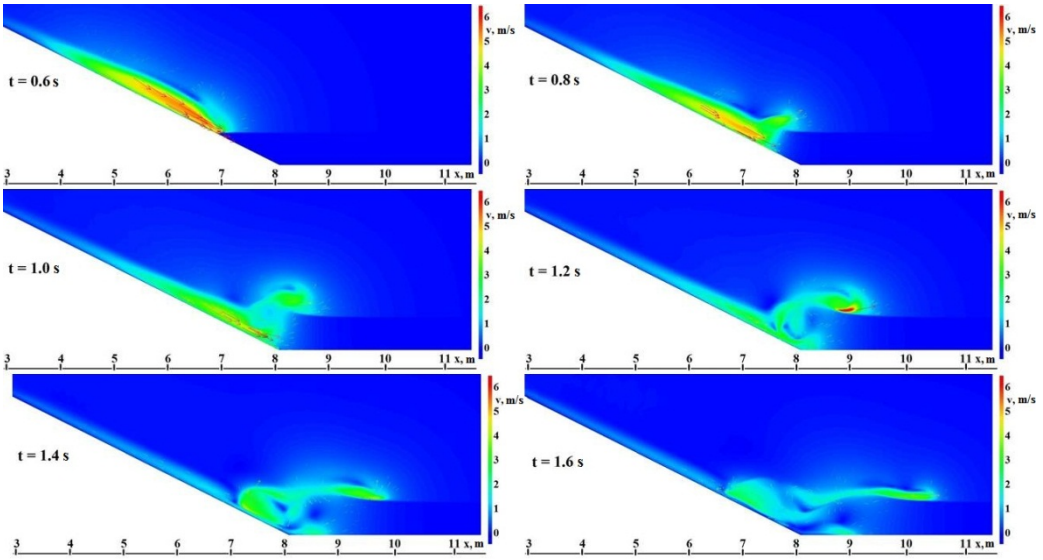

Fig. 4. The fluid velocity field at different times

The simulation is carried out with automatic selection of the time step in accordance with the given Courant number equal to unity. The pattern of the landslide entry into the water and its spread to the barriers is the same for both configurations. So, the following result presentation refers to configuration 1. Fig. 4 shows the velocity field at different points in time of the landslide entering the water. The figure shows that at the time of entry into the water (t = 0.6 s), the landslide has a speed of about 5.5 m/s, which is in good agreement with the experiment. The maximum medium speed is observed for the water phase at the wave breaking point (t = 1.2 s) and is greater than 6 m/s.

The velocity distribution pattern also allows us to see air disturbances which are very low (about 1 m/s) as compared with the other phases, which legalizes that air compressibility ca be neglected. At the overturn moment the wave has the amplitude of about 50 cm that corresponds to the water displacement in the basin (Fig. 5).

After the first wave overturn, the landslide still continues moving along the bottom. After the main mass sliding at the time of 2 sec the second wave with the amplitude 2 times smaller than the first is formed. At the time of 4 sec the landslide is completely in the water, and two waves move on its surface one after the other. At time point of 6 sec a wave runup on the artificial "fiords" is observed. Their amplitude is about the same and is about 10 cm (Fig. 6). The wave runup is also observed on the "fiords" from which the landslide occurred, and its magnitude is about the same.

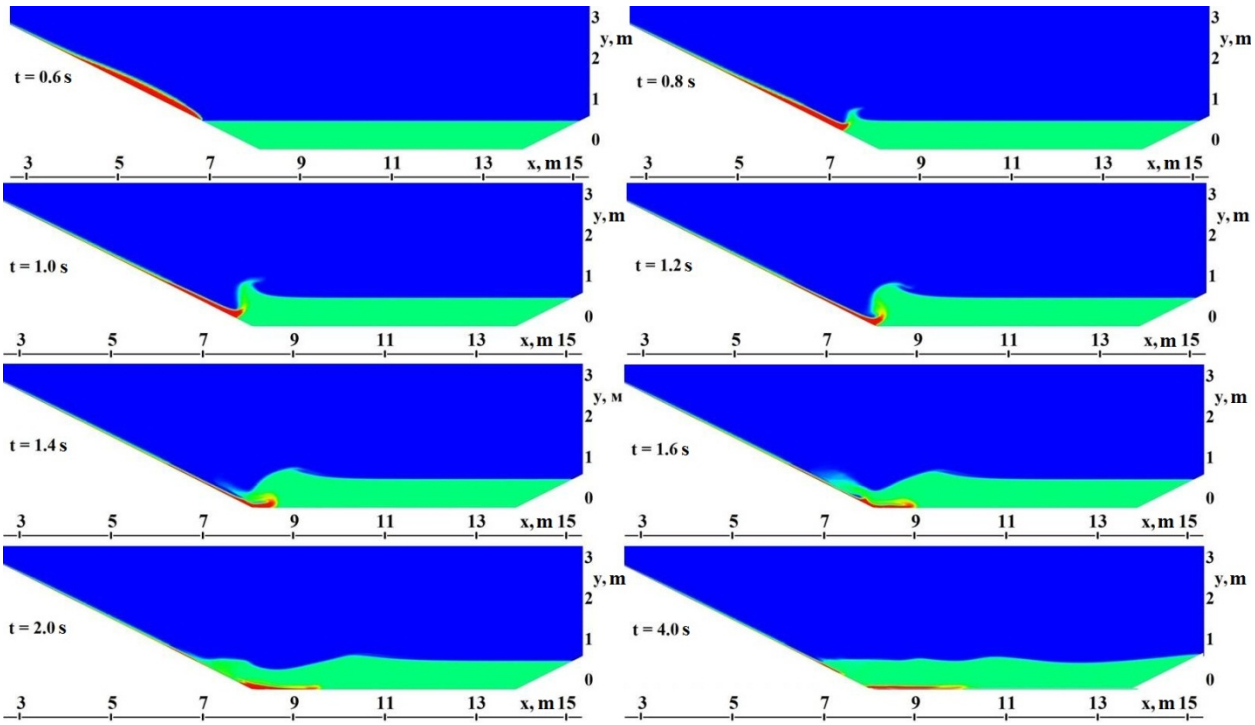

Fig. 5. Snapshots of water displacement in the basin at different times

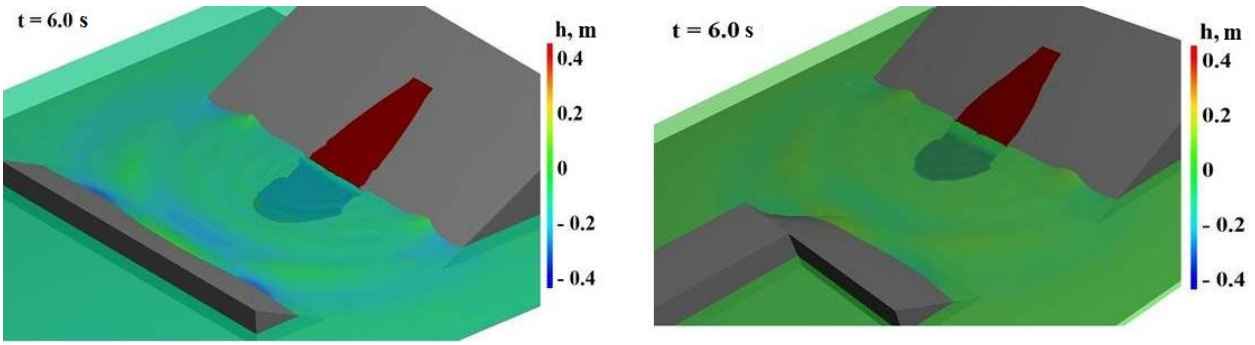

Fig. 6. Wave pattern (left – configuration 1, right – configuration 2)

The computed quantitative characteristics of a wave pattern in the tank can be estimated by tide-gauge data (Figs 7 and 8). As can be seen from the figures, numerical calculation reproduces the tide-gauge records of all the incoming waves, and their amplitude is almost identical with that obtained in the experiment. This applies to both the first wave and the last waves. The only significant difference in the numerical experiment is obtained for tide-gauge 1 in configuration 1 for the "averaged" incoming waves. In the numerical calculation, the re-reflection wave processes strengthened its amplitude even more than it was observed in the experiment. In the experiment there is also a certain gain, although much weaker. For fiord 2 all tide-gauges also gave a good agreement on the wave pattern. The slight difference in wave heights is observed for the third tide gauge.

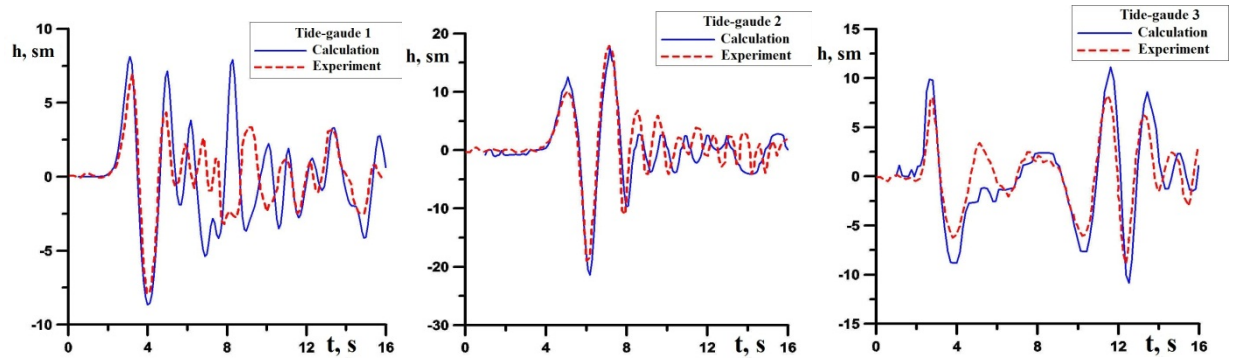

Fig. 7. Tide-gauge records for configuration 1

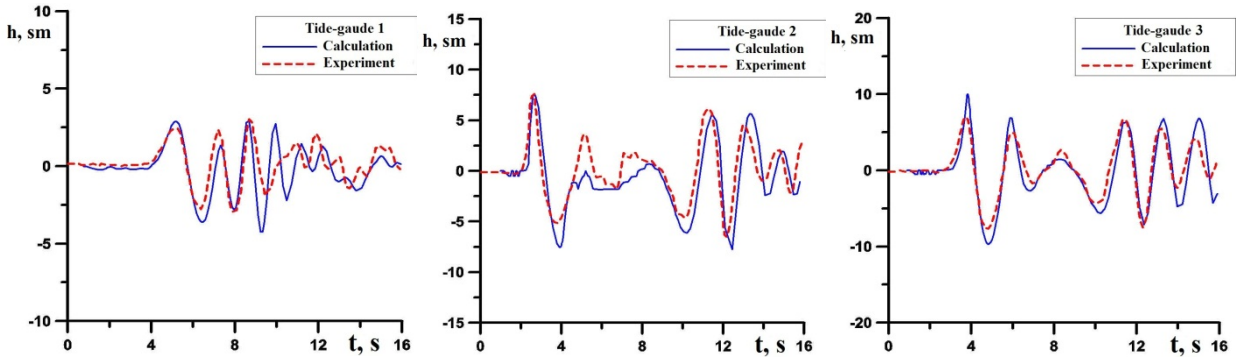

Fig. 8. Tide-gauge records for configuration 2

3.2. Underwater landslide simulation

Here we use the results of (Langford, 2007; Grilli et al, 2003; Watts, et al., 2001) which describe a series of experiments on partially submerged landslides. Schematically, the tank configuration is shown in Fig. 9.

The landslide starts free sliding down on an inclined plane at an angle of 15^0. During the experiment the surface displacement is measured at several tide-gauge points located on a water surface at a certain distance from the shore.

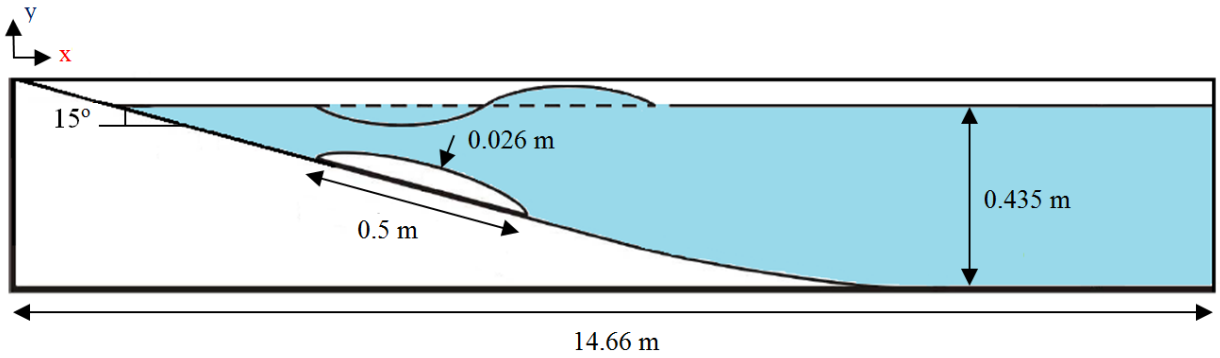

Fig. 9. Tank configuration to study underwater landslide

The experimental configuration SG3_IS5 is chosen for the study, according to which the landslide density is 2830 kg/m^3, the water and air parameters are set in accordance with the values of Table 1. For the modeling the same type computational grid is used as for the surface landslide (Fig. 3), consisting of ~ 100,000 cells. In the area of the landslide movement and wave propagation the grid has a thickening to describe the landslide motion and flow characteristics more accurately. The water depth is 0.435 m, the tank length is 14.66 m. The inclined plane along which the landslide moves is set by the equation

$$f(x)=\begin{cases} -x\cdot\tan(15^0),\ 0\le x\le 1.297\ \text{m},\\ 0.19\cdot(x-1.297)^3+0.1024\cdot(x-1.297)^2-0.2728\cdot(x-1.297)-0.3475,\ 1.297\ \text{m}\le x\le 1.807\ \text{m},\\ -0.435,\ \ 1.807\ \text{m}\le x\le 14.66\ \text{m}. \end{cases}$$

In this case the landslide dimensions are 0.5 m × 0.026 m × 0.25 m. The initial landslide position is also set according to the selected configuration (half-emerged state), with its mass located at a distance of 0.19 m from the coast and at a depth of 0.1 m below the water level (Fig. 10).

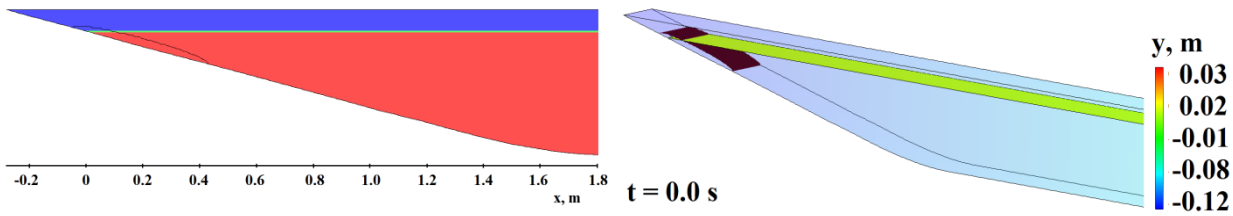

Fig. 10. Landslide location at the initial time

The simulation is carried out with time step automatic selection with the given Courant number equal to 0.5. The pattern of the landslide into the water, its moving along the inclined plane and wave propagation is observed in the time interval of 7 sec. After the first wave overturn the landslide continues moving along the inclined bottom (Fig. 11).

After the main mass sliding at one time moment of 1.6 sec the second wave is formed with the amplitude smaller than the first. At the point of time of 2.6 sec the landslide is completely in the water and successive waves move on its surface.

The quantitative characteristics of the waves can be found from the tide-gauge data (Fig. 12). Here tide gauge 1 is located at a distance of 1.5 m, tide gauge 2 - at a distance of 2.5 m, tide gauge 3 - at a distance of 3.5 m, and tide gauge 4 - at a distance of 4.5 m (all distances from the left boundary). Computed and observed wave amplitudes are almost the same. This applies to both the first and the last waves. Only strengthening (weakening) of the second wave is observed. The most significant difference in the numerical experiment is obtained for tide-gauge 1 for the "first" negative and the "second" positive incoming waves. In the numerical calculation re-reflection processes more strengthened/weakened the wave than is observed in the experiment. The experiment also has a certain gain, although much weaker. On the whole, the simulation results well correlate with the experimental data.

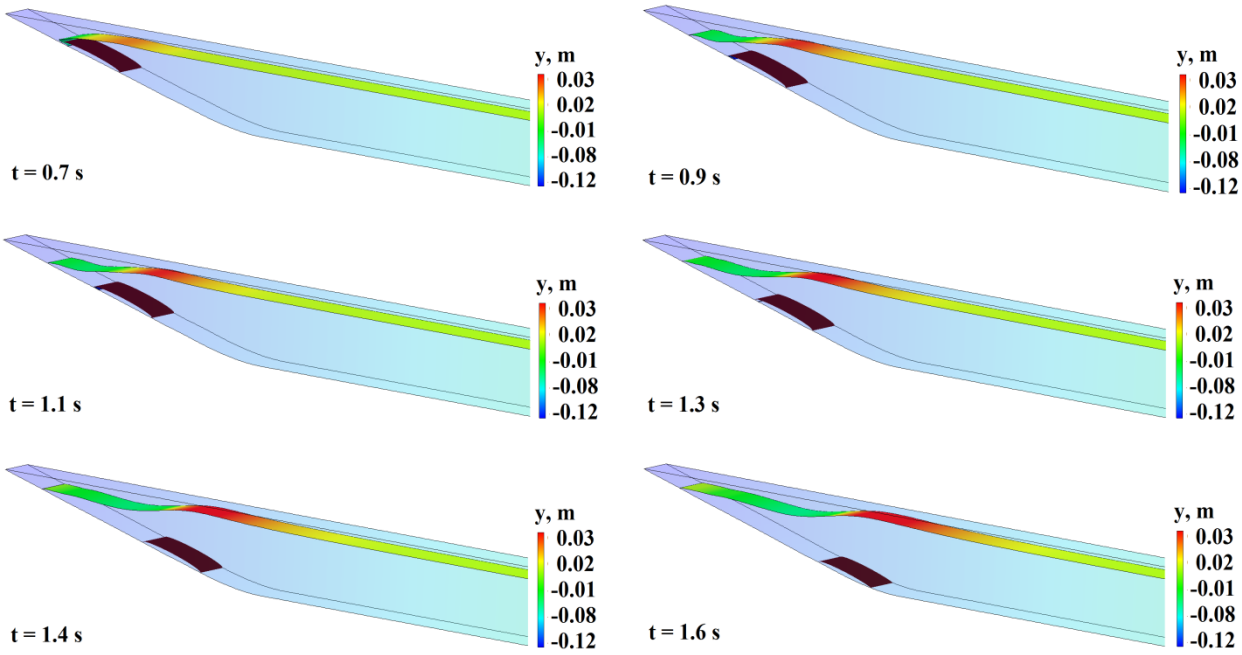

Fig. 11. Snapshots of landslide motion and wave propagation

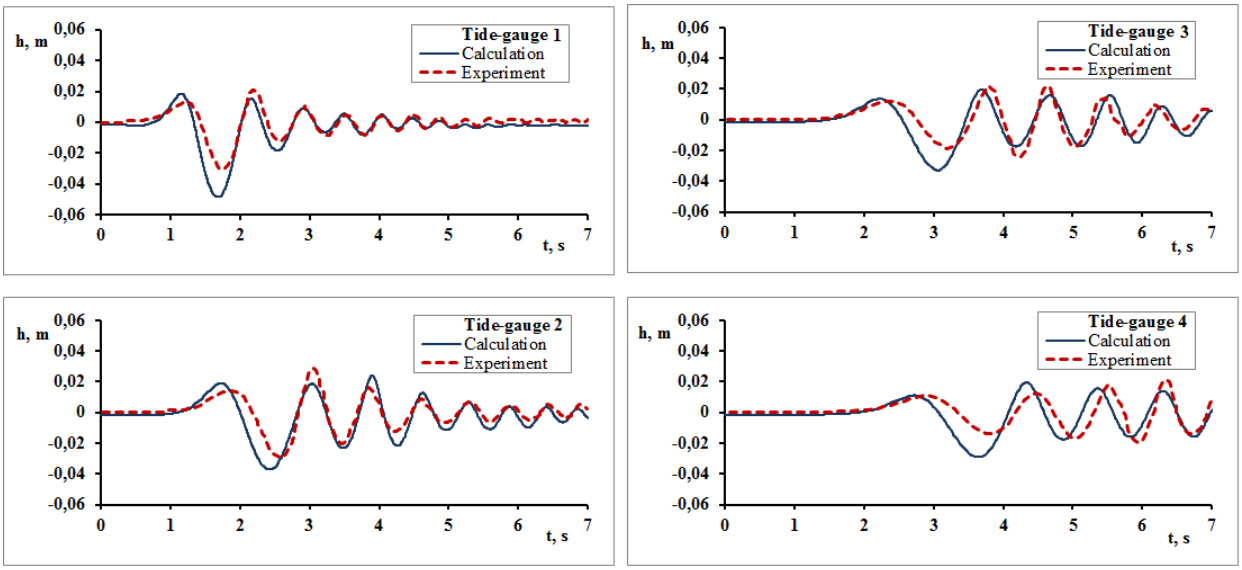

Fig. 12. Tide-gauge records

4. GRID PATTERN CONSTRUCTION TECHNOLOGY

Building a grid model for the numerical solution of the Navier-Stokes equations is one of the key and most difficult stages of the entire modeling process. The experience of solving various classes of problems shows (Kozelkov et al, 2016; Betelin et al., 2014) that the grid model construction can take more than 70% of the time beginning with the task up to obtaining the final result. The quality of the constructed grid directly depends on the accuracy of the solution. The most universal type of grid models are unstructured grids consisting of arbitrary shape polyhedra. The level of development of unstructured grid automatic generators allows building a grid model of the required quality in the field of arbitrarily complex geometric configuration in a relatively short time. Automatic generation means choosing the average grid cell size for the entire computational domain, which ultimately results in a major drawback of this method – the size of the final grid model can reach enormous sizes (hundreds of millions and even billions of counting cells). Therefore, the use of this generator type involves the introduction of sub-areas of the grid model with its own size and then their aggregation. In addition, this grid type imposes restrictions on the used numerical schemes. Then the order of approximation schemes, as a rule, does not exceed the second order unless special methods to increase accuracy are used (Volkov et al., 2014). In addition, the classical scheme of the second order of the central-difference type on such grids are completely unstable, and to make calculations on their basis it is necessary to build a hybrid scheme adding a share of counter-flow (Jasak, 1996; Ferziger & Peric, 2001; Kozelkov et al, 2016; Kozelkov & Kurulin, 2015). Despite all the difficulties, these grids are essential for most industrial-oriented tasks, and at present they are an integral part of the technological chain of the process of mathematical modeling.

Another way to build a grid model is the use of block-structured grids. When constructing them, it is possible to control the size of the cells and their growth rate in a given direction, and, therefore, to control their quantity. The advantage of this method is the ability to use high-order accuracy schemes due to pre-known grid model structure. A significant disadvantage of this method is that the construction of acceptable quality grid patterns in the areas of complex geometric configuration may require the introduction of a substantial number of units and their further conjugation. It results in back-breaking manual labor that can last for months. If a total pattern can allocate large blocks which enable building a block- structured grid, it is advantageous to do so. The current practice of hydrodynamic calculations often uses a combination of block- structured and automated approaches.

When the Navier- Stokes equations are used in tsunami problems, it is expedient to resort to the combination of the two presented approaches. This is primarily due to the different scales of the considered tsunami stages as well as wave characteristics. It should be stressed that this applies to all types of tsunamis, modeled by using the Navier-Stokes equations: seismic, cosmogenic and landslide origin. For the seismic-origin tsunami the different scales of the source and propagation area are not as critical as, for example, for cosmogenic and landslide origin, as the size of the seismic source can amount to tens of kilometers. In this case, the cell size in the area of the tsunami generation and propagation is comparable. For cosmogenic and landslide tsunamis the situation is different. Cosmogenic tsunami generation can be caused by a meteorite of only a few meters large (Kozelkov & Pelinovsky, 2016; Kozelkov et al., 2015), whereas wave propagation is thousands of kilometers. Grid pattern sell dimensions in the area of meteorite movement is times (and, perhaps, dozens of times) different from the cell size in the tsunami propagation area.

This is also characteristic of landslide-origin tsunami, though, perhaps, with less stringent requirements, since the landslide size however large, is unlikely to amount to tens of kilometers. Also, when modeling the landslide motion it is necessary to take into account the force of friction on the "underlying" surface. It involves the selection of the boundary layer for calculating it accurately by analogy with the turbulent boundary layer (Kozelkov et al, 2015, 2016; Kozelkov & Kurulin, 2015).

In addition, to describe tsunami wave propagation in the ocean where the wave amplitude amounts to tens of centimeters, it is necessary to use a grid with about the same cell size. Given, that the ocean depth can be hundreds of meters and grid generation with cell size of tens of centimeters will lead to a grid model of enormous size, it is advisable to apply the mechanism of cell size thickening of the grid model to the interface "air water". All these considerations are the basis of unstructured grid model construction technology for tsunami wave simulation on the basis of the Navier-Stokes equations presented below.

Let us consider landslide-origin tsunami near the island of Montserrat in the Caribbean based on the works of (Pelinovsky et al, 2004; Heinrich et al., 2001). The calculation area highlighting landslide (area 1) and tsunami propagation sub-domains (area 2) is shown in Fig. 13.

The bathymetric map of the area of the Lesser Antilles, Caribbean is downloaded from the website of the International Data Centre for Digital Bathymetry [https://www.ngdc.noaa.gov]. When building a grid model, accounting bathymetric data is carried out by excluding from calculation the cells located below the earth's surface bathymetric line and the ocean floor. To do this, the whole bathymetric model is immersed in a box with the correct dimensions exceeding the size of the model. Then the

extra cells are simply removed. This method of constructing the computational model includes 3 stages:

- the construction of a computational grid with a flat bottom, the depth of which is determined by the maximum depth of the considered water area section according to bathymetric data;
- the calculation of the local water depth for the coordinates of the each calculated cell center by interpolating the data from the next bathymetric points;
- the exclusion from the calculation model the cells, the vertical coordinate of which lies below the bottom.

Fig. 13. Calculation domain of highlighting landslide (area 1) and tsunami propagation (area 2)

This technology is simple to implement, but it leads to a step change in the level of the water area bottom (Fig. 14) which is determined by the characteristic cell dimension near the bottom, and can be reduced by local refinement of the computational grid. Obviously, the smaller the grid near the bottom is, the more accurately it describes the bathymetric line. After the procedure provided, a surface grid describing the bathymetric relief of the earth's surface and the ocean floor is formed on the basis of a set of bathymetric points.

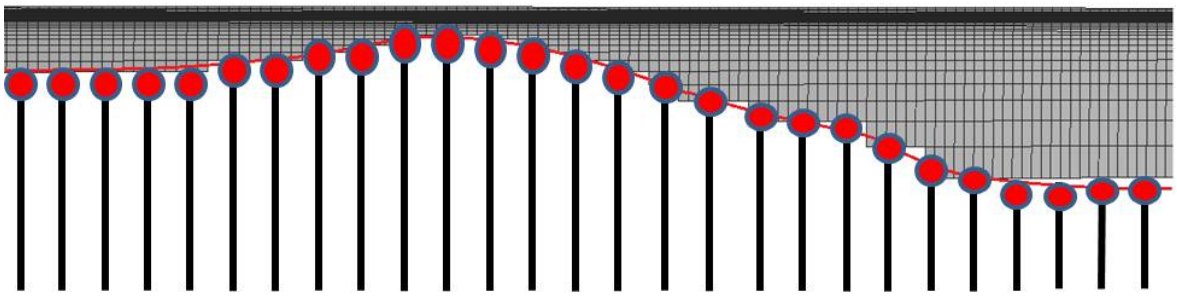

Fig. 14. Computational grid near the bottom, the line is bathymetric line built on the basis of map points (●)

To construct a grid in the landslide area (area 1 in Fig. 13) is used an automatic unstructured grid generator with highlighting the prismatic boundary layer. Using the boundary layer allows to describe the landslide rheology and the frictional force between the landslide and the underlying surface more accurately. It is assumed that at the initial time the landslide has a parallelepiped shape with dimensions 800×2000×25 m in width, length and height, respectively (Fig. 15). This corresponds to the parameters set out in [52, 57] and the volume of pyroclastic flow descended into the sea is 40×10^{6} $м^{3}$

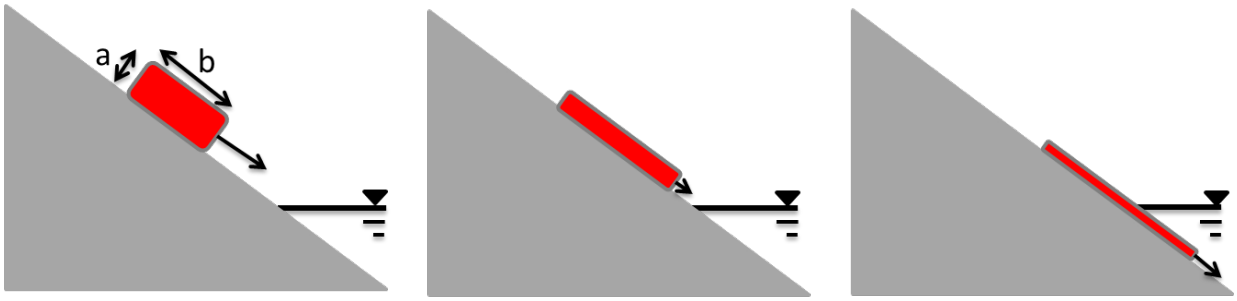

Fig. 15. Landslide motion

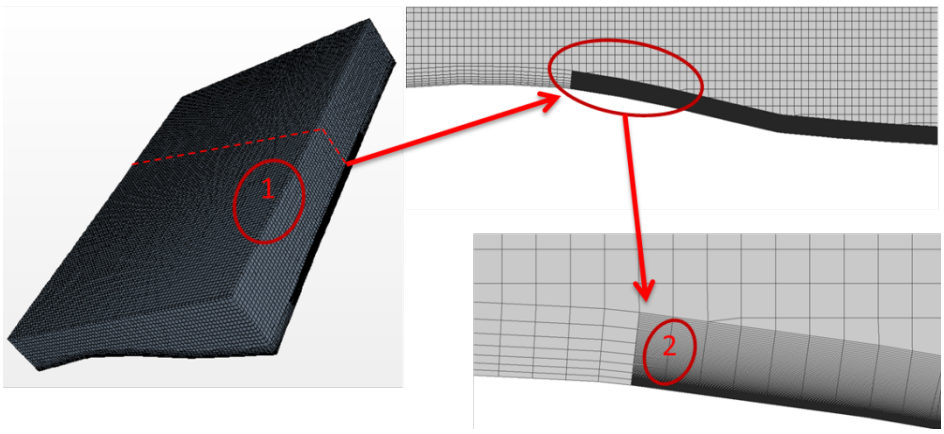

Fig. 16. Grid model for the pyroclastic flow gathering field

In this case, the input data for the grid generator is a surface grid area 1 (Fig.13). The specification of a slope surface in the pyroclastic formation area is achieved by using a refinement unit for the boundary layer. The width of the boundary layer is about 30 meters (dimension "a" in Fig.15). This value is slightly higher than the maximum height of the pyroclastic flow at the initial time and allows simulating it the necessary detailing. When needed, this value can be increased or decreased in accordance with the required dimensions of the modeled landslide, i.e. the size of the refinement unit is set out considering the pyroclastic flow initial position and its motion size range. With these parameters, the base cell size is 75 m (Fig. 16, area 1). In the zone of the boundary layer considering the first refinement, the near-wall cell height is 1 m (Fig.16, area 2) with 1.15 growth factor. Fig. 16 (right) shows an enlarged fragment of the section in the zone of the refinement unit. These grid resolution parameters are optimized for the geometry of the problem and can adequately simulate all the features of the pyroclastic flow movement and its entry into the water, thus creating a pulse provoking a tsunami wave. The size of the grid model of the pyroclastic flow gathering (area 1 in Fig.13) contains about 7 million cells.

In the open ocean, where it is necessary to simulate tsunami propagation, it is advisable to build a block-structured grid specifying the interface of "water-air" section. The main purpose of constructing the grid in such a way is thus providing a sufficient size cells near the interface of the "water-air" section in the entire area for simulating both energy-bearing and fading tsunami waves of small amplitude. With the help of the block-structured grid generator is built a regular parallelepiped with dimensions 230 km × 230 km, the depth of 5200 m and 1100 m height (it is determined by the maximum depth and the height of the area under consideration according to the bathymetric data) (Fig.13, area 2). Since the pyroclastic gathering detailing area is not taken into account, from the main block a parallelepiped is cut whose coordinates coincide with the coordinates of the block for area 1 (Fig.13). The methodology of interface separation is as follows. After building the model geometry, a three-dimensional block is divided on its edge into 2 parts. The main coordinate of the rib is aligned with the surface of the "water-air" section ($z = 0$). The linear dimension of the cells adjacent to the top and bottom of "water-air" interface is 0.1 m. This size is specified increasing by the law of geometrical progression with the growth rate from the surface to the bottom and to the top interface of the air by a factor of 1.15. This allows to get rid of too "small" cells in the areas that do not require simulation. The thickening of the "water-air" section interface is shown in Fig. 17 left. In addition, the area is divided into blocks of additional cell refinement near the dock to provide a smooth transition from the small cell size in the detailing area to a bigger size in the area of the free wave propagation (Fig.17, right).

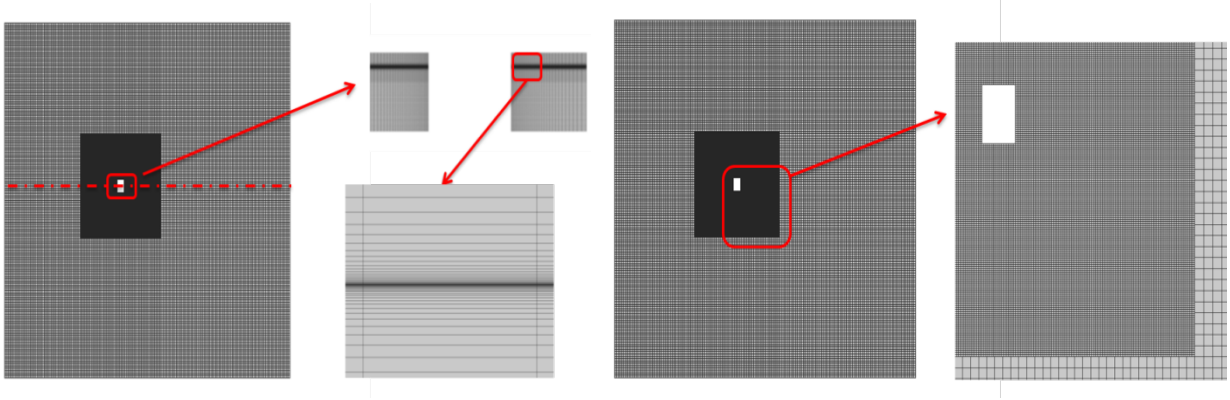

Fig. 17. Computational grid block with interface “water – air” condensation (left) and a transition area between the grid blocks (right)

Next, according to the algorithm described above, the accounting of bathymetric data is carried out by excluding the cells, located below the earth’s surface bathymetric line and the ocean floor, from the computational domain. Thus constructed the grid model for area 2 contains approximately 13 million cells, i.e., the general model consisting of these two areas will contain about 20 million cells. To construct the final grid model the grids, obtained in the previous two stages, are to be linked. To do this, both grid models are loaded in the LOGOS pre-post-processor package. Further, both grids are united into one using the node connection procedure (Fig. 18). Figure 18 below shows an enlarged fragment of the section in the joining zone of the two grid models.

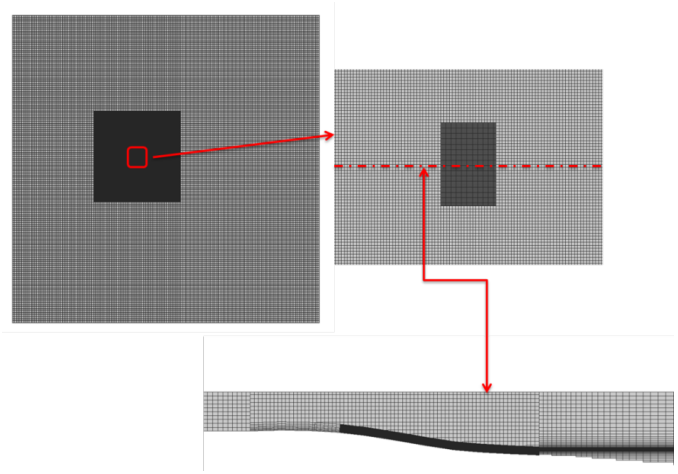

Fig. 18.The final grid model for the computational domain

Thus, the presented technology of this class grid building provides an adequate quality grid model, which consists mostly of regular hexahedral cells with adequate resolution for numerical simulation of both the pyroclastic flow gathering area and the propagation of waves of varying amplitude. It should be noted here that this technology allows constructing grid models for a more accurate calculation of tsunami runup. To do this a coast zone must be selected and a grid constructed by an automatic

generator in the same way as for area 1 in Fig. 13. The selection of the boundary layer in the runup area allows not only setting the desired properties of the underlying surface (roughness accounting with special boundary conditions), but also simulating the turbulent wave transformation in the collapse by the method of wall functions.

5. TECHNOLOGY TO ACCELERATE THE COMPUTATIONS

In many practical problems the discretization of the Navier-Stokes equations yields a system of difference equations with ill-conditioned matrix, the condition number of which is often 10^7-10^8, but for some cases it may be close to 10^{10} (Kozelkov et al., 2013, 2016). As a result, that the matrix SLAE decision is the most costly step. When using classical iterative methods it takes about 90% of the calculated step computing time. These classical iterative methods either do not work or give a very slow rate of convergence. One way to accelerate convergence and improve the stability of the iterative process is a multigrid method (Tai & Zhao, 2003; Volkov et al, 2013; Kozelkov et al., 2013, 2016), based on the use of a sequence of nested grids and transition operators from one grid to another. Here the algebraic and geometric approaches are distinguished. In the algebraic approach the discrete equation of the sequence of nested grids are formed without constructing nested grids on the matrix level, whereas in the geometric approach – the hierarchy of networks created by merging the control volumes of the upper level of the grid (the detailed one). It is easy to build grid levels using original matrices generated by implicit discretization of the Navier-Stokes equations. It leads to the simplicity of building operators of restriction and continuation thus making the algebraic approach very attractive from a computational point of view. The geometric method requires additional algorithms of rebuilding the computational grid which can be justified for certain classes of problems. Advantages and disadvantages of both approaches are discussed in (Volkov et al., 2013).

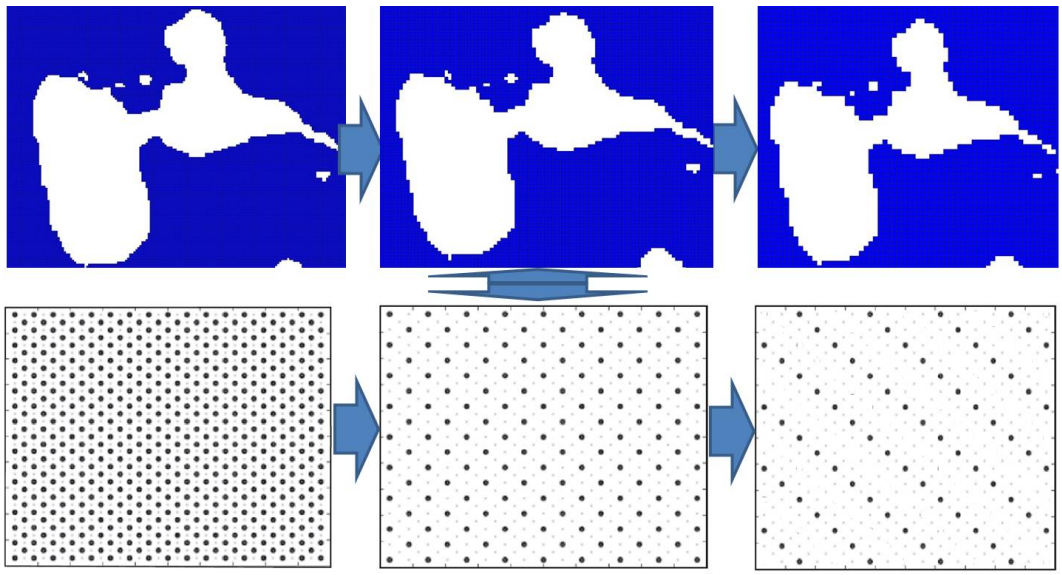

Fig. 19. The sequence of nested grids in the matrix (below) and grid levels (top)
(the top of the figure shows Guadeloupe, Lesser Antilles, Caribbean)

The construction of an algebraic multigrid method for geophysical problems involves automatic coarsening of the original grid on the matrix level (Fig. 19). The calculation of the equation (12) using a multigrid method is as follows. Equation (12) can be represented in the general form:

$$A_h x^h = b^h, \tag{16}$$

where h is the index of discrete equation belonging to h grid. The interpolation operator P from a coarse grid H on a detailed grid h allows you to represent the operator A_H on the coarse grid in the form of

$$A_H = R\, A_h\, P, \tag{17}$$

where $R = P^T$. The solution correction step is as follows:

$$x^h_{new} = x^h_{old} + Pe^H\,. \tag{18}$$

The solution correction e^H is an exact solution of the equation

$$A_H\, e^H = r^H, \tag{19}$$

where $r^H = R\, r^h$, $r^h = b^h - A_h x^h_{old}$.

Thus, the multigrid method using solution correction scheme represents the following sequence of steps (Fig. 20, left):

1. μ_1 solution approximations on the grid h by using the Zeidel method (pre-smoothing) are done.

2. The residual $r^h = b^h - A_h x^h_{old} \in V_h$ is projected onto the space V_H, т.е. $r^H = Rr^h$.

3. The approximate solution $A_H\, e^H = r^H$ on the coarse grid is found. γ multigrid cycles are done recursively for this.

4. The correction e^H is interpolated on a detailed grid and decision correction is made on the detailed grid $x^h_{new} = x^h_{old} + Pe^H$.

5. μ_2 decision approximations are done on the detailed grid to suppress interpolation errors (final smoothing)

Depending on the number of recursive method calls γ on each grid level emit different types of cycles are singled out. When $\gamma = 1$ there is a V-cycle, if $\gamma = 2$ – there is a W-cycle (Fig. 20, right). If at each level is recursively called one a W-cycle, and then the a V-cycle , we obtain an F- cycle (Kozelkov et al., 2015).

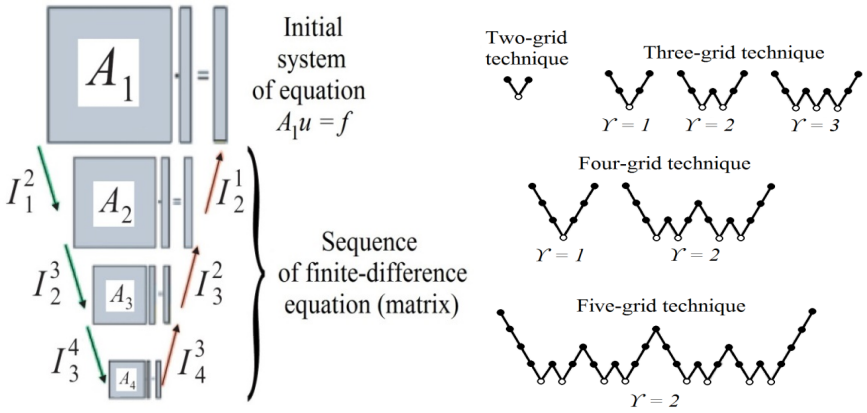

Fig. 20. Matrix sequence (left) and the V- and W- cycles (right)

In the aggregation method of coarsening with constant interpolation all variables divided into I_k units containing all the indices i, which correspond to the cells included in the unit k. The operator construction on the coarse grid is produced by the relation:

$$A_H = RA_hP = \left(a_{kl}^H\right), \quad a_{kl}^H = \sum_{i \in I_k} \sum_{j \in I_l} a_{ij}^h, \ (k, l \in C). \tag{20}$$

The multigrid method parallelization implies that the matrix coarsening during the transition from one level to another occurs independently on each MPI-process (Kozelkov et al., 2016a,b). The coarsening process in parallel mode creates two problems. Firstly, the coarsening is stopped if in each the process there is one left. Secondly, on a gross level where the matrix dimension is small the time spent on the inter-processor communication, due to communication environment latency, begins to repeatedly exceed computed time. To solve these problems (Kozelkov et al., 2016) suggests performing the collection of small matrices in one process, forming one global level and continuing coarsening and solution in sequential mode (Fig. 21, left).

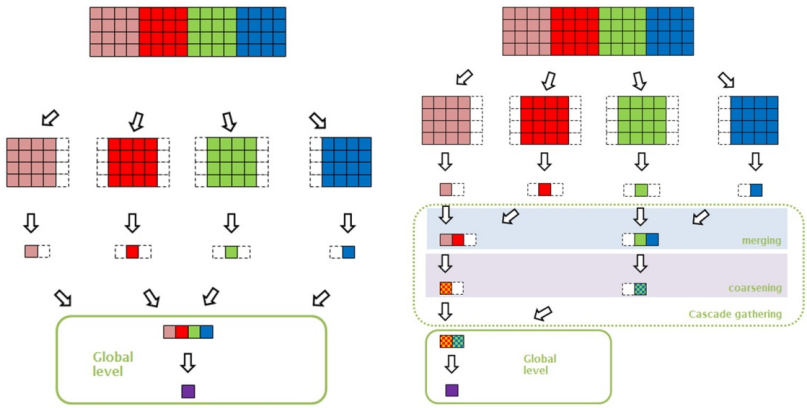

Fig. 21. Global level formation (left) and its cascading collection (right)

Using a global level can complete the coarsening process in a parallel case, and also, can avoid the overhead expenses resulting from inter-processor communication in the coarse grid level processing because of the global level storage on one process. The analysis of the proposed algorithm effectiveness, held in (Kozelkov et al., 2016), showed that the average time of computations increasing as compared with the classical iterative methods is 4-6 times. A major shortcoming of the global level is that it is performed in a sequential mode. When determining the amount of the problem, the memory of the unit on which the main processor is located may not be enough to build a global level. This aspect will also affect the limitation of the algorithm when using large-scale grids of hundreds of millions of cells (such grids are typical of geophysical problems). The way out here is the use of cascading level algorithm to gradually reduce the number of processes involved in the analysis while maintaining the advantages of the global level. The cascading level algorithm is also presented in (Kozelkov et al., 2016). It includes the stage of breaking the whole initial set of residual matrix after coarsening in pairs and performing their twinning. In the second stage the operation is repeated until the total coarse level matrix is obtained (Fig. 21, right). The level consolidation level in itself, in addition to generating information on a new level, contains a procedure of re-definition information about inter-processor exchanges, which also requires spending some of the CPU time. In addition, the parallel procedure of cascade level coarsening requires the introduction of additional inter-processor communication, which are absent in the case of scalar implementation at the global level collection.

The main advantage of the cascade summation scheme is the algorithm scalability. It actually removes restriction on the maximum size of the problem to be solved because of the possible lack of memory unit on which the global level is developed. Furthermore, the global level speed increases since its component parts are formed and coarsened independently.

6. TSUNAMI SIMULATION

6.1. Tsunami from the “model” source

To verify the performance of the presented methodology was simulate the tsunami propagation in the one part of the World Ocean. It is based on the tsunami generated by the slide of the pyroclastic flow into the water resulting from the eruption of the Soufriere Hills Volcano on Montserrat, Caribbean (Pelinovsky et al., 2004). In (Pelinovsky et al., 2004) this tsunami modeled by using two approaches. In the first case the model cone-shaped source was used as initial approximation, and the wave propagation was computed using the code TUNAMI (Goto et al., 1997) (recommended by UNESCO for tsunami research), which is based on shallow-water theory. In the second case the pyroclastic flow was generated by the model described in (Watts & Waythomas, 2003) and the propagation was computed by the code FUNWAVE (Kirby et al., 1998) based on the nonlinear-dispersive theory. Later, after adding the block to calculate different initial perturbations this code got the name

GEOWAVE. In (Pelinovsky et al., 2004) is shown quite a significant difference in the results obtained using these approaches both in predicting wave heights and wave pattern as a whole. It is also noted there that non-linear dispersion theory is more preferable to use. Taking into account that hydrodynamic cone-shaped source (Fig. 22,a) was used in (Pelinovsky et al., 2004) for both calculations as an initial tsunami approach, here, to compare tsunami propagation adequately, was taken a source generated by the model described in (Watts & Waythomas, 2003). The source produced by this model is also cone-shaped (Fig. 22,b). Its geometric parameters correspond to the descended pyroclastic flow. The amplitude of the initial wave in the tsunami source is 1.26 m. The distance between the nodes of the computational grid has a resolution of 500 m. Fig. 23 shows the comparison of wave patterns produced by different approaches (here is the comparison only with the GEOWAWE code (the wave pattern with use the TUNAMI program is similar). As you can see, qualitatively, the pictures are practically identical.

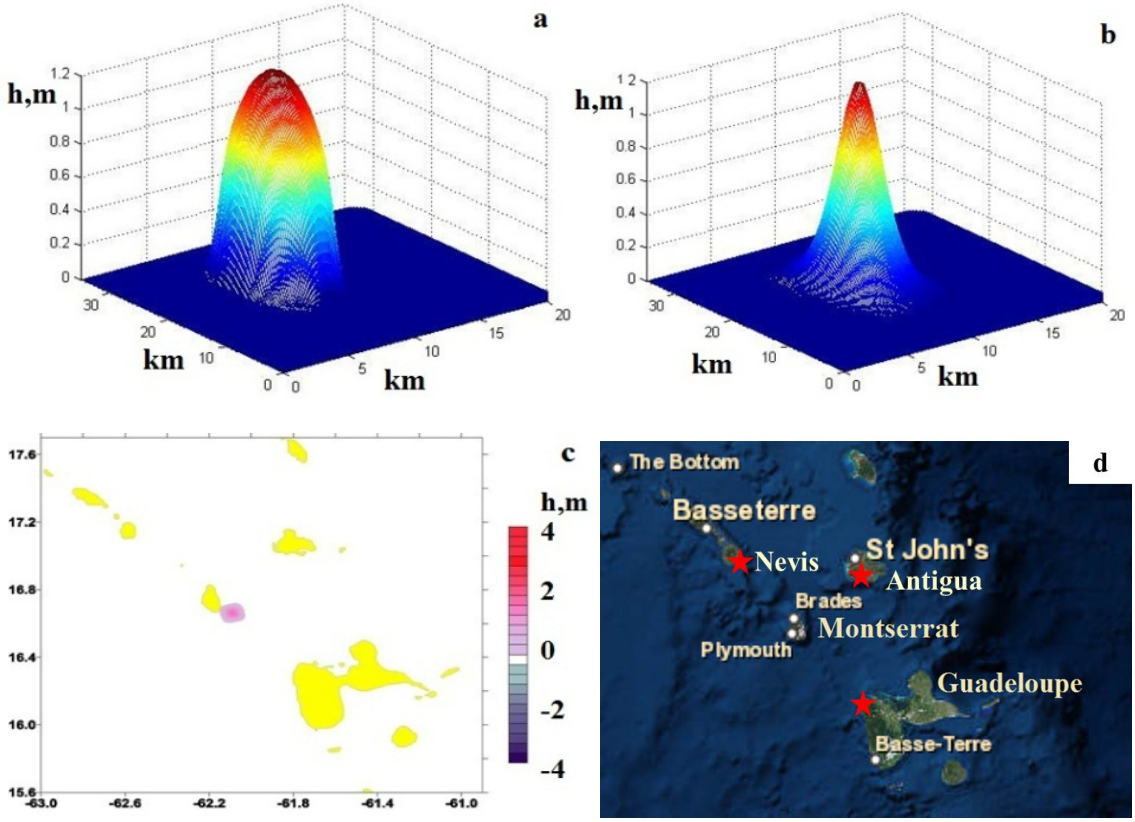

Fig. 22. Tsunami source: *a* – hydrodynamic source; *b* – source gained by code GEOWAVE; *c* – computation domain; *d* – the location of gauges

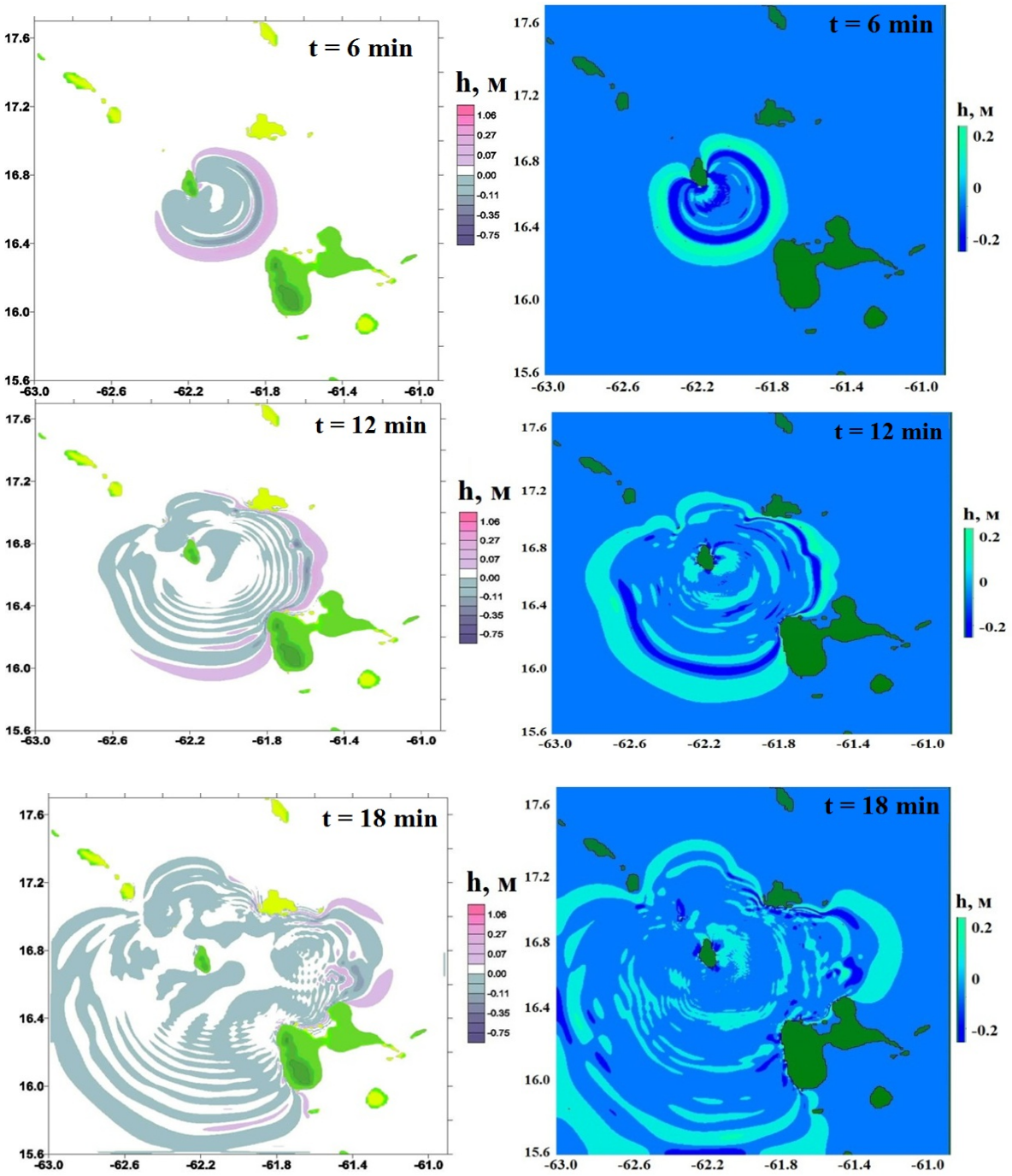

Fig. 23. Snapshots of tsunami propagation: GEOWAVE (left) and LOGOS (right)

Quantitative comparison of tide-gauge records shown in Fig. 24 can also be considered very satisfactory. The leading waves that came in the north-western part of the island of Guadeloupe and

the island of Antigua are almost identical. The first three waves are predicted by both calculations, though they have slightly different heights. Subsequent waves are described differently, and the Navier-Stokes equations give a more pronounced oscillatory character, while the waves calculated by nonlinear-dispersive shallow-water theory fade quicker. These differences may be related to many factors and require further study. These factors include primarily the models themselves - they are different and are solved by various numerical approaches - finite differences and finite volumes. The secondary factors include grid model resolution and numeric approximation schemes.

Here should be noted the temporal characteristics of the calculations. The grid model for programs based on the shallow water and nonlinear dispersive equations are always two-dimensional with a fixed height above sea level at each computational point. The total number of points is only about 200 million (the grid is 430×430). With the help of these models on the grid only tsunami propagation is calculated which requires about 3 hours of computer time opposed to 40 minutes of physical time on a single processor. The LOGOS software package carries out the numerical solution of the Navier-Stokes equations exclusively in three-dimensions. In the three-dimensional grid, taking into account topographic features, tsunami propagation requires within 40 minutes of physical time about 15 hours on 96 processors. So, the computation is 5 times longer than two-dimensional and occupies 100 times greater volume of CPU field. The difference can be explained by the models used. The above-mentioned two-dimensional models only describe the wave propagation and do not allow supplementing by source and runup calculation. In this regard, the three-dimensional model based on the Navier-Stokes equations is more versatile - it includes the presence of these stages, and does not limit the physical properties of propagation such as viscosity, dispersion and nonlinearity. Expectedly, in any in any case, the Navier-Stokes equations reproduce the process more accurately, but they require more resources than such simplified models as the shallow water equations.

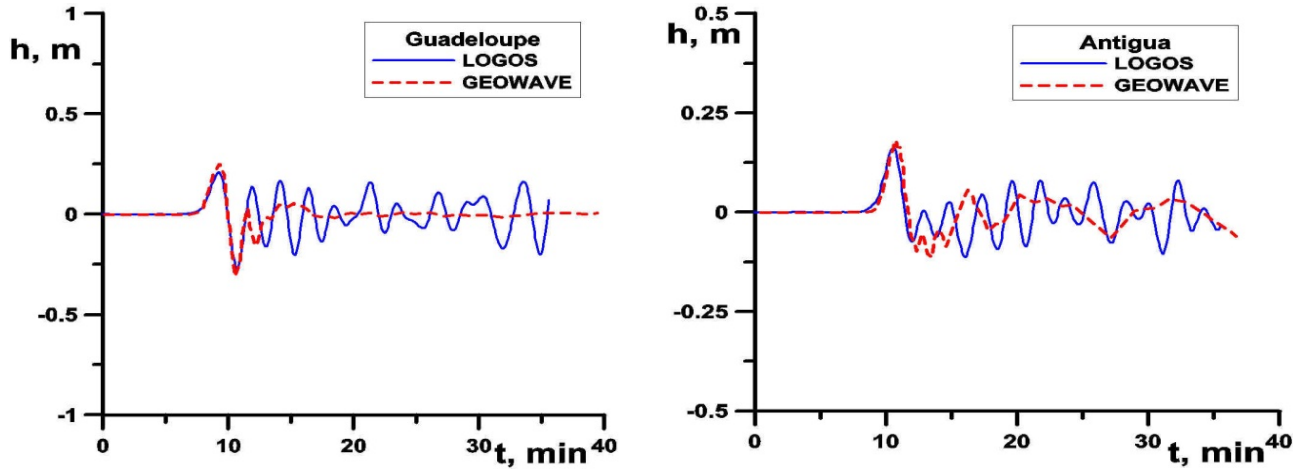

Fig. 24. Comparison of tide-gauge records on Guadeloupe and Antigua

6.2. Tsunami with the simulated slide of the pyroclastic flow

To generate a tsunami directly by pyroclastic flow slide a multi-phase system of the Navier-Stokes equations and the method described in Section 2 will be used. In this problem setting the landslide is modeled as a Newtonian fluid with its physical characteristics. The properties of all system phases correspond to Table 1 (Section 3). The grid model, the technology of its construction and the geometric parameters of the computational area the landslide are described in Section 4. The movement of the pyroclastic stratum is due to gravity, the initial velocity is absent. The input speed of a landslide in the water as well as sea-level in the same gauges is recorded. The simulation is carried out with the automatic selection of the time step in accordance with the given Courant number equal to 1. Figure 25 presents the velocity field at different moments of the landslide entering the water. The figure shows that at the time of entering the water (t = 10 c) the landslide has a speed of about 25-30 m/s. The landslide maximum speed is observed at the moment of it entering the water (t = 30 c) and exceeds 35 m/s. The velocity pattern also allows seeing the disturbance of the air, which are negligible in comparison with the other phases. This fact proves air compressibility neglect justified.

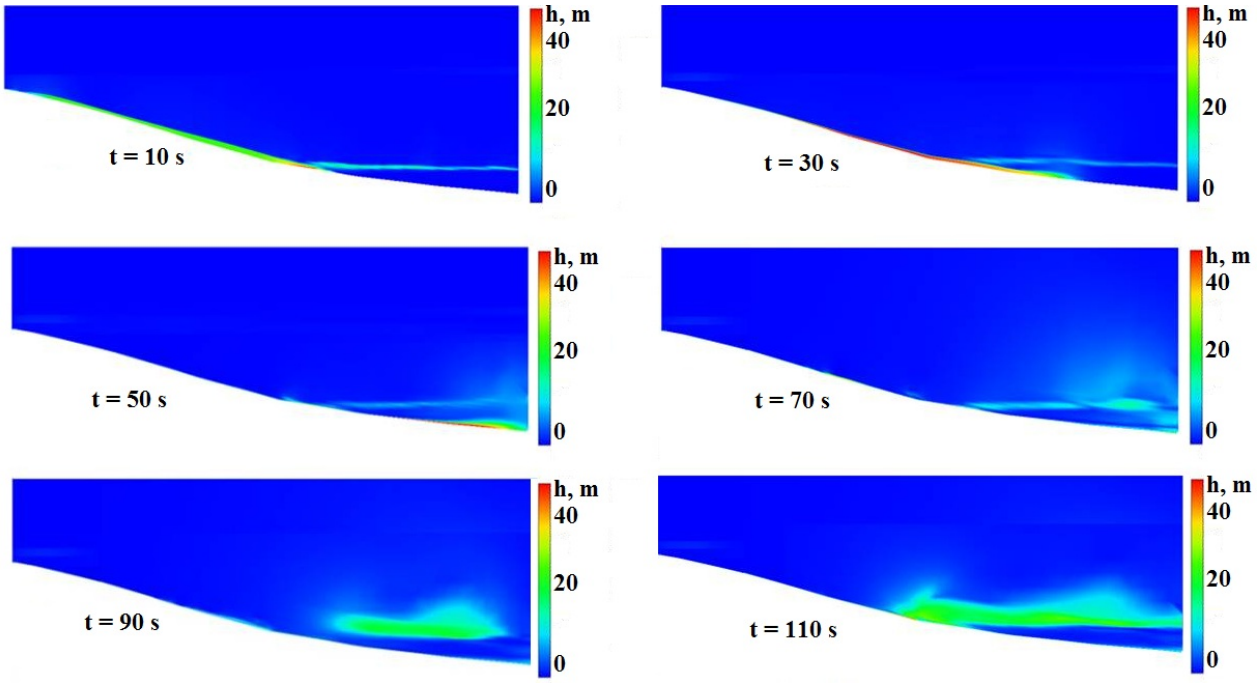

Fig. 25. Snapshots of velocity of the multiphase system at the landslide entering the water (on the axes are marked meters)

Figure 26 demonstrates 3D view of wave pattern in the entrance area of the landslide. As you can see, the model based on the Navier-Stokes equations gives a more detailed picture of the landslide motion than the previously discussed models (Fig. 22,a and 22,b), and can essentially give a comprehensive

picture of the landslide tsunami source. Moving along the side of the mountain, the landslide takes the form of its topography precisely fitting all its features. About a minute later the landslide completely enters the water, at the same time a tsunami wave is generated. The wave height at the source is high enough and reaches 20 meters, which is equal to the data (Heinrich et al., 2001).

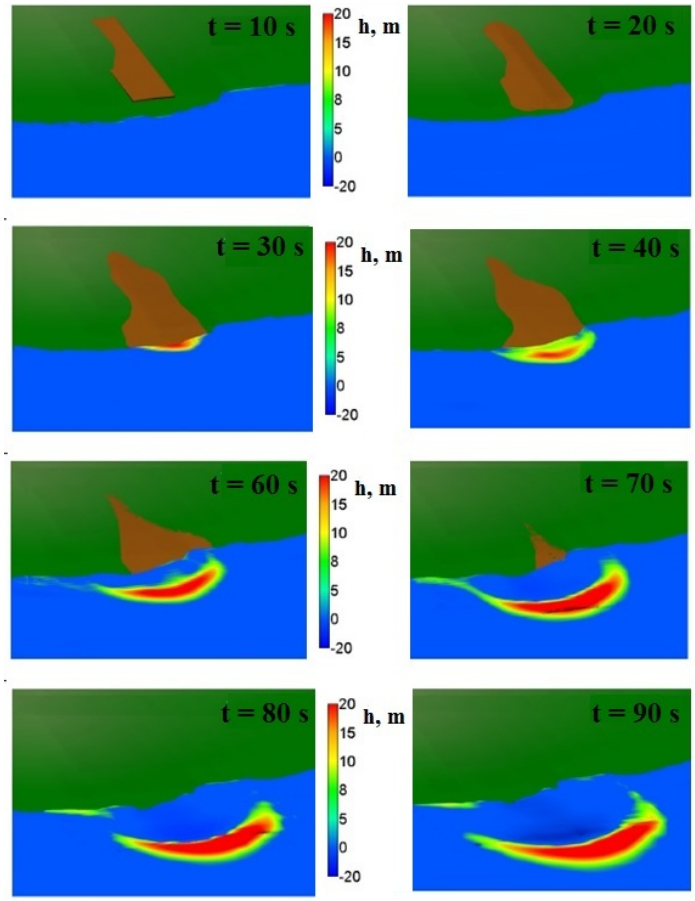

Fig. 26. 3D view of the entrance area

Figure 27 shows a further development of 3D wave perturbations. Here secondary waves departing from major wave at the source can be observed. These are edge waves propagating along the shoreline, and their amplitude is small as compared with the main source of the disturbance. All this points to the capabilities of the model used to describe complex fluid physics. Wave propagation in the Caribbean is shown in Fig. 28. It is next to impossible to define the difference in the wave pattern between the three models used.

It should be recalled that the grid model used in these calculations is built with a detailed landslide area and consists of about twenty million three-dimensional cells. On this grid tsunami propagation for 40 minutes of physical is calculated for about 72 hours on 320 processors when using the implicit integration method of the Navier-Stokes equations. It is 5 times longer than a similar 3D calculation with a model source and 12 times longer than the 2D calculation. It takes 320 times bigger processor

field as compared with the 2D calculation and more than 3 times bigger as compared with the 3D calculation, but with the model source. This increase in the time of the calculation can be accounted for by the detailed entrance area of the landslide. However, the latter made it possible not only to track the movement of the landslide on the slope, but also to identify additional physical aspects of a tsunami generation formed by a pyroclastic flow slide.

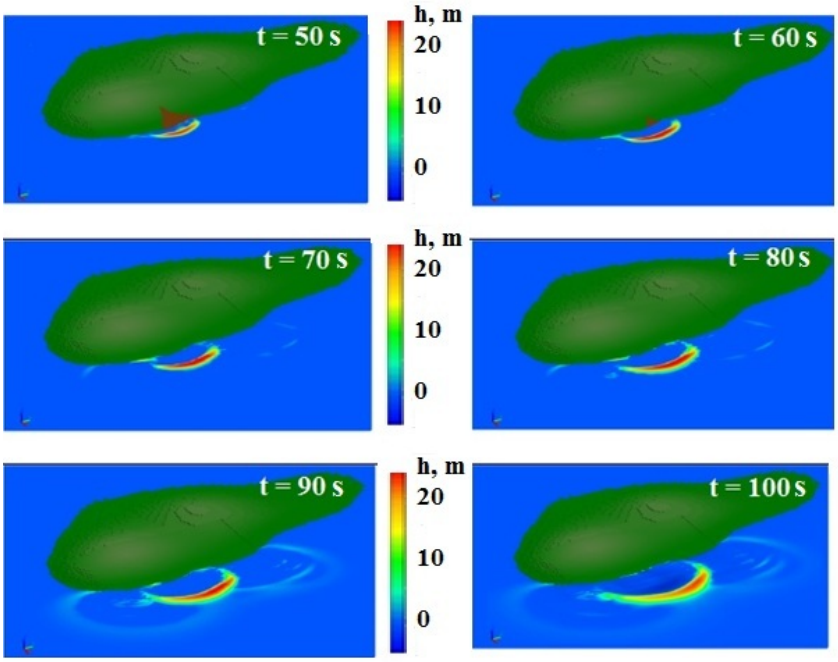

Fig. 27. Snapshots of 3Dl wave pattern with detailed wave disturbances

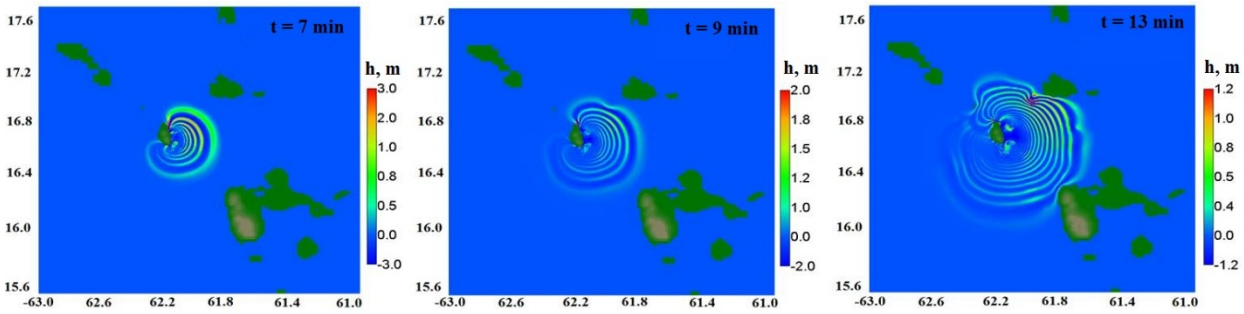

Fig. 28. Snapshots of tsunami propagation

Figure 29 demonstrates the comparison of tide-gauge records in the framework of the Navier-Stokes equations with a pyroclastic flow slide (LOGOS), shallow-water equations (TUNAMI) and nonlinear-dispersive equations (GEOWAVE). The first waves that came on the north-western part of the island Guadeloupe differ greatly. The wave height computed by the LOGOS is twice higher, which better agrees with observations. The gauges «OldRoad» located on the island of Antigua shows a higher

result, which better agrees with reality as the island is in close proximity to Montserrat, and there has to be one of the peaks. The gauges on Nevis Island, located on the opposite side from the eruption site, shows at once a fading wave. The result obtained by LOGOS is closer to the result obtained by the shallow-water equations. Nonlinear-dispersive equations give much greater attenuation (fading). Subsequent waves are described in different ways, and the Navier-Stokes equations give a more pronounced oscillatory character, while the waves, calculated by the nonlinear-dispersion model, also fade faster.

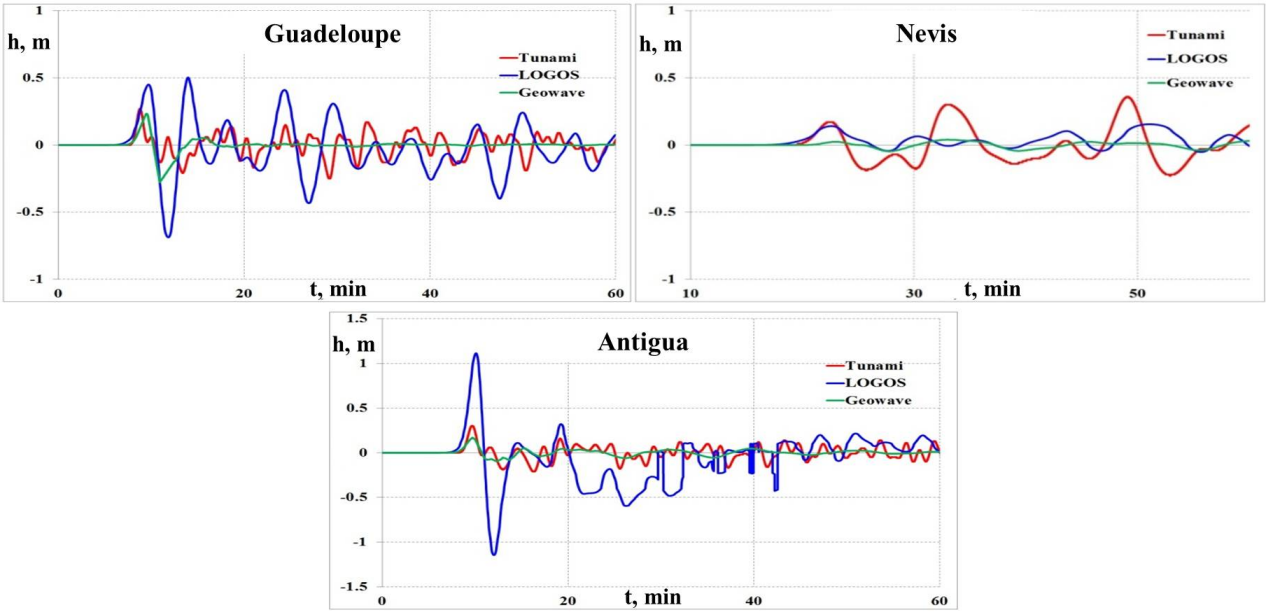

Fig. 29. Comparison of tide-gauge records according to three models

As a result, all the models show that in the north-western part of the island of Guadeloupe a tsunami wave is generated, although the shallow-water and nonlinear-dispersive theories show a more modest result in amplitude. The model based on the Navier-Stokes equations is much closer to the observations (Pelinovsky et al, 2004). It is not difficult to guess and, it really is obvious, that it all depends on the description of the tsunami source. The Navier-Stokes equations reproduce the landslide tsunami source more accurately.

7. CONCLUSION

The paper describes the technology for computations the landslide-origin tsunami based on the Navier-Stokes equations. The landslide source is modeled by a separate phase representing a Newtonian fluid with its own density and viscosity. The methodology of numerical solution of multiphase system is based on a fully implicit method, which removes strict restrictions on the time step, and allows simulating tsunami propagation at arbitrarily large distances. The formulas for

discretization of equation sampling and coefficient types are given. To effectively calculate tsunami propagation in large water areas is presented an algorithm based on an algebraic multigrid method. The results of a full-scale experiment calculation are given. They demonstrate the possibility of using computed technology provided all stages of the landslide-origin tsunami - generation, propagation and runup. The algorithm to account bathymetric data for tsunami simulation in real waters of the World Ocean is described. The technology of building 3D grid models with the detailed area of generation and runup is demonstrated. The results of the comparison with the nonlinear- dispersive theory on the example of the historical tsunami of volcanic origin are presented, which showed a fairly good agreement for identical sources but different results for the parametric source and the actual slide.

ACKNOWLEDGEMENTS

The presented results were obtained with the financial support of the grants of the President of the Russian Federation for state support of leading scientific schools of the Russian Federation (NSH-6637.2016.5) and with the financial support of the RFBR grants 16-01-00267, 15-45-02961.

REFERENCES

1. Beizel, S.A., Chubarov, L.B. and Khakimzyanov, G.S. Simulation of surface waves generated by an underwater landslide moving over an uneven slope // Russ. J. Numer. Anal. Math. Modelling, 2011, vol. 26, no. 1, 17-38.

2. Betelin, V.B., Shagaliev, R.M., Aksenov, S.V., Belyakov, I.M., Deryuguin, Yu.N., Kozelkov, A.S., Korchazhkin, D.A., Nikitin, V.F., Sarazov, A.V. and Zelenskiy, D.K. Mathematical simulation of hydrogen–oxygen combustion in rocket engines using LOGOS code // Acta Astronautica 2014, vol. 96, 53-64.

3. Cecioni, C. and Bellotti, G. Modeling tsunamis generated by submerged landslides using depth integrated equations // Applied Ocean Research, 2010, vol. 32, 343-350.

4. Chen, Z.J. and Przekwas, A.J. A coupled pressure-based computational method for incompressible/compressible flows // J Computational Physics, 2010, vol. 229, 9150-9165.

5. Chin Hoe Tai and Zhao Yong. Parallel unsteady incompressible viscous flow computations using an unstructured multigrid method // J Computational Physics, 2003, vol. 192, 277-311.

6. Didenkulova, I., Nikolkina, I., Pelinovsky, E. and Zahibo, N. Tsunami waves generated by submarine landslides of variable volume: analytical solutions for a basin of variable depth // Natural Hazards and Earth System Sciences, 2010, vol. 10, 2407-2419.

7. Didenkulova, I.I., Nikolkina, I.F. and Pelinovsky, E.N. Resonant amplification of tsunami waves from an underwater landslide // Doklady Earth Sciences, 2011, vol. 436, no. 1, 66-69.

8. Dutykh, D. and Dias, F. Energy of tsunami waves generated by bottom motion // Proc. R. Soc. A, 2009, vol. 465, 725-744.

9. Fedotova, Z.I., Chubarov, L.B. and Shokin, Y.I. Simulation of surface waves caused by landslides // Vycisl. tehnologii – Computational Technologies, 2004, vol. 9, no. 6, 89-96 [In Russian].

10. Ferziger, J.H. and Peric, M. Computational methods fluid dynamics. 3rd edition. – Berlin; Heidelberg; New York; Barcelona; Hong Kong; London; Milan; Paris; Tokyo: Springer, 2002. 423 p.
11. Fine, I.V., Rabinovich, A.B., Bornhold, B.D., Thomson, R.E. and Kulikov, E.A. The Grand Banks landslide-generated tsunami of November 18, 1929: preliminary analysis and numerical modeling // Marine Geology 2005, vol. 215, 45-57.

12. Fritz, H.M., Mohammed, F. and Yoo, J. Lituya Bay Landslide Impact Generated Mega-Tsunami 50th Anniversary // Pure Appl. Geophys., 2009, vol. 166, 153-175.

13. Goto, C., Ogawa, Y., Shuto, N. and Imamura, N. Numerical method of tsunami simulation with the leap-frog scheme (IUGG/IOC Time Project), IOC Manual, UNESCO, no. 35, 1997, 96 p,

14. Grilli, S.T., Vogelmann, S. and Watts, P. Development of 3D numerical wave tank for modeling tsunami generation by underwater landslides // Engineering Analysis with Boundary Elements, 2002, vol.26, 301-313.

15. Grilli, S.T., Kirby, J.T., Liu, P.L.F., Brandes, H. and Fryer, G.J. «Workshop on Model Validation and Benchmarking For Tsunami Generation by Submarine Mass Failure - Proposal Submitted to NSF», 2003, Honolulu, Hawaii.

16. Gusev, O.I., Shokina, N.Y., Kutergin, V.A. and Khakimzyanov, G.S. Numerical modelling of surface waves generated by underwater landslide in a reservoir // Vycisl. tehnologii – Computational Technologies, 2013, vol. 8, no. 5, 74-90 [In Russian].

17. Harbitz, C.B., Løvholt, F., Pedersen, G. and Masson, D.G. Mechanisms of tsunami generation by submarine landslides: a short review // Norwegian Journal of Geology, 2006, vol. 86, 255-264.

18. Hirt, C.W. and Nichols, B.D. Volume of Fluid (VOF) method for the dynamics of free boundaries // Journal of Computational Physics, 1981, vol. 39, 201-225.

19. Heinrich, P., Schindele, F., Guibourg, S. and Ihmle, P. Modeling of the February 1996 Peruvian tsunami // Geophys. Res. Lett. 1998, vol. 25, no. 14, 2687-2690.

20. Heinrich, F., Boudon, G., Komorowski, J.C., Sparks, R.S.J., Herd, R. and Voight, B. Numerical simulation of the December 1997 debris avalanche in Montserrat // Geophys. Research Letters, 2001, vol. 28, 2529-2532.

21. Horrillo, J., Wood, A., Kim, G.B. and Parambath, A. A simplified 3-D Navier-Stokes numerical model for landslide-tsunami: Application to the Gulf of Mexico // Journal of Geophysical Research: Oceans, 2013, vol. 118, 6934-6950.

22. http://tsun.sscc.ru/hiwg (accessed 3 July 2015).
23. https://www.ngdc.noaa.gov (accessed 25 April 2015).

24. Imamura, F. and Imteaz, M.A. Long waves in two-layers: Governing equations and numerical model // Science of Tsunami Hazards, 1995, vol. 13, no. 1, 3-24.

25. Jasak, H. Error Analysis and Estimation for the finite volume method with applications to fluid flows. Thesis submitted for the degree of doctor. – London: Department of Mechanical Engineering, Imperial College of Science, 1996.

26. Kirby, J., Wei, G., Chen, Q., Kennedy, A. and Dalrymple, R. Fully Nonlinear Boussinesq Wave Model Documentation and Users Manual // Center for Applied Coastal Research Department of Civil Engineering University of Delaware, Newark DE 19716, Research Report №. CACR-98-06, 1998.

27. Kolev, N. Multiphase Flow Dynamics. – Berlin, Heidelberg: Springer-Verlag, 2007.

28. Kozelkov, A.S., Deryugin, Yu.N., Lashkin, S.V., Silaev, D.P., Simonov, P.G. and Tyatyushkina, E.S. Implementation in LOGOS software of a computational scheme for a viscous incompressible fluid using the multigrid method based on an algorithm SIMPLE // VANT. Ser.: Mat. Mod. Phys. Proc., 2013. no. 4, 31-43. [In Russian]

29. Kozelkov, A.S., Kurkin, A.A., Pelinovsky, E.N., Kurulin V.V. and Tyatyushkina, E.S. Modeling the Disturbances in the Lake Chebarkul Caused by the Fall of the Meteorite in 2013 // Fluid Dynamics, 2015, vol. 50, no. 6, 828-840.

30. Kozelkov, A.S. and Kurulin, V.V. Eddy resolving numerical scheme for simulation of turbulent incompressible flows // Computational Mathematics and Mathematical Physics, 2015, vol. 55, no. 7, 1255-1266.

31. Kozelkov, A.S., Kurkin, A.A., Legchanov, M.A., Kurulin, V.V., Tyatyushkina, E.S. and Tsibereva, Y.A. Investigation of the application of RANS turbulence models to the calculation of nonisotermal low-Prandtl-number flows // Fluid Dynamics, 2015, vol. 50, no. 4, 501-513.

32. Kozelkov, A.S., Kurkin, A.A., Pelinovsky, E.N. and Kurulin V.V. Modeling the cosmogenic tsunami within the framework of the Navier–Stokes equations with sources of different types // Fluid Dynamics, 2015, vol. 50, no. 3, 306-313.

33. Kozelkov, A., Kurulin, V., Emelyanov, V., Tyatyushkina, E. and Volkov, K. Comparison of convective flux discretization schemes in detached-eddy simulation of turbulent flows on unstructured meshes // Journal of Scientific Computing, 2016a, vol. 67, 176-191.

34. Kozelkov, A.S., Shagaliev, R.M., Kurulin, V.V., Yalozo, A.V. and Lashkin S.V. Investigation of Supercomputer Capabilities for the Scalable Numerical Simulation of Computational Fluid Dynamics Problems in Industrial Applications // Computational Mathematics and Mathematical Physics, 2016b, vol. 56, no. 8, 1506-1516.

35. Kozelkov, A. and Pelinovsky, E. Tsunami of the meteoritic origin // In Book «Dynamics of Disasters - key Concepts, Models, Algorithms, and Insights», Eds: Kotsireas I.S. et al., Springer Proceedings in Mathematics & Statistics 185, Berlin: Springer, 2016. DOI 10.1007/978-3-319-43709-5_8

36. Langford, P.S. Modeling of tsunami generated by submarine landslides. PhD Thesis. – New Zealand: University of Canterbury, 2007.

37. Liu, P.L.-F., Wu, T.-R., Raichlen, F., Synolakis, C.E. and Borrero, J.C. Runup and rundown generated by three-dimensional sliding masses // J. Fluid Mech., 2005, vol. 536, 107-144.

38. Lynett, P. and Liu, P.L.-F. A numerical study of the run-up generated by three-dimensional landslides // Journal of Geophysical Research, 2005, vol. 110, C03006.

39. Lynett, P. Hydrodynamic Modeling of Tsunamis Generated by Submarine Landslides: Generation, Propagation, and Shoreline Impact // 4-th International Symposium Submarine Mass Movements and Their Consequences, Advances in Natural and Technological Hazards Research, 2010, vol. 28, 685-694.

40. Ma, G., Kirby, J.T. and Shi, F. Numerical simulation of tsunami waves generated by deformable submarine landslides // Ocean Modelling, 2013, vol. 69, 146-165.

41. Macías, J., Vázquez, J.T., Fernández-Salas, L.M., González-Vida, J.M., Bárcenas, P., Castro, M.J., Díaz-del-Río, V. and Alonso, B. The Al-Borani submarine landslide and associated tsunami. A modelling approach // Marine Geology, 2015, vol. 361, 79-95.

42. Mohammed, F. and Frits, H.M., Experiments on tsunamis generated by 3D Granular Landslides // Submarine Mass Movements and Their Consequences, Advances in Natural and Technological Hazards Research, 2010, vol. 28, 705-718.
43. Mohammed, F. Physical Modeling of tsunamis generated by three-dimensional deformable granular landslides. PhD Thesis. – Atlanta: Georgia Institute of Technology, 2010.
44. Nikolkina, I.F., Pelinovsky, E.N. and Talipova, T.G. Nonlinear dynamics of gravity flows in sloping channels // Doklady Earth Sciences, 2010, vol. 432, pt. 2, 812-815.
45. Okal, E. and Synolakis, C.E. A Theoretical comparison of tsunamis from dislocations and landslides // Pure Appl. Geophys., 2003, vol. 160, 2177-2188.

46. Papadopoulos, G.A. and Kortekaas, S. Characteristics of Landslide Generated Tsunamis From Observational Data // Submarine Mass Movements and Their Consequences Advances in Natural and Technological Hazards Research., 2005, 367-374.
47. Pelinovsky, E.N. Analytical models of tsunami generation by submarine landslides // In NATO Science Series, ed. by A. Yalciner et al., Earth Environ. Sci., 21, Kluwer, Dordrecht, Boston 2003, 111-128.

48. Pelinovsky, E., Kozelkov, A., Zahibo, N., Dunkly, P., Edmonds, M., Herd, R., Talipova, T. and Nikolkina, I. Tsunami generated by the volcano eruption on July 12-13, 2003 at Montserrat, Lesser Antilles // Science of Tsunami Hazards, 2004, vol. 22, no. 1, 44-57.

49. Rabinovich, A.B., Thomson, R.E., Bornhold, B.D., Fine, I.V. and Kulikov, E.A. Numerical modelling of tsunamis generated by hypothetical landslides in the Strait of Georgia, British Columbia // Pure Appl. Geophys., 2003, vol. 160, 1273-1313.

50. Rhie, C.M. and Chow, W.L. A numerical study of the turbulent flow past an isolated airfoil with trailing edge separation // AIAA, 1983, vol. 21, 1525-1532.

51. Sælevik, G., Jensen, A. and Pedersen, G. Experimental investigation of impact generated tsunami; related to a potential rock slide, Western Norway // Coastal Engineering, 2009, vol. 56, 897-906.

52. Ubbink, O. Numerical prediction of two fluid systems with sharp interfaces. PhD Thesis. – London: Department of Mechanical Engineering Imperial College of Science, Technology & Medicine, 1997.

53. Volkov, K.N. and Emelyanov, V.N. Particle laden flows. – Moscow: Fizmatlit, 2008. 600 p. [In Russian].

54. Volkov, K.N., Deryugin, Yu.N., Emelyanov, V.N., Karpenko, A.G., Kozelkov, A.S. and Teterina, I.V. Methods of the detached eddy for gas-dynamic calculation on unstructured grids. – Moscow: Fizmatlit, 2013. 536 p. [In Russian].

55. Volkov, K.N., Deryugin, Yu.N., Emelyanov, V.N., Kozelkov, A.S. and Teterina, I.V. Difference schemes in problems of gas dynamic on unstructured grids. – Moscow: Fizmatlit, 2014. 416 p. [In Russian].

56. Watts, P., Grilli, S.T., Kirby, J.T., Fryer, G.J. and Tappin, D.R. Landslide tsunami case studies using a Boussinesq model and a fully nonlinear tsunami generation model // Natural Hazards and Earth System Sciences, 2003, vol. 3, 391-402.

57. Watts, P. and Grilli, S.T. Underwater landslide shape, motion, deformation, and tsunami generation // Proc. of the 13th Intern. Offshore and Polar Eng. Conf., Honolulu, Hawaii, 2003, vol. 3, 364-371.

58. Waclawczyk, T. and Koronowicz, T. Remarks on prediction of wave drag using VOF method with interface capturing approach // Archives of civil and mechanical engineering, 2008, vol. 8, 5-14.

59. Watts, P., Imamura, F., Bengston, A. and Grilli, S.T. Benchmark cases for tsunamis generated by underwater landslides // Proceedings of the Fourth International Symposium Waves, San Francisco, 2001, 1505-1514.

60. Watts, Ph. and Waythomas, C.F. Theoretical analysis of tsunami generation by pyroclastic flows // Journal of Geophysical Research, 2003, vol. 108, no. B12, 21 p.

61. Zahibo, N., Pelinovsky, E., Talipova, T. and Nikolkina, I. The Savage-Hutter model for the avalanche dynamics in inclined channels: analytical solutions // J. Geophys. Res., 2010, vol. 115, B03402.